Estimation of path attenuation and site characteristics in the north-west Himalaya and its adjoining area within Indian Territory using generalized inversion method

Harinarayan, NH[1], Abhishek Kumar[*2]

[1, 2] Department of Civil Engineering, Indian Institute of Technology Guwahati, Assam, India.

Corresponding to: Kumar Abhishek (abhitoaashu@gmail.com/ abhiak@iitg.ernet.in)

Abstract. Present work focuses on the determination of path attenuation and site characteristics of earthquake recording stations, located in the north-west Himalaya and its adjoining region, within India. The work is done using two-step generalized inversion technique. In the first step of inversion, non-parametric attenuation curves are developed. $Q_s = (105 \pm 11)f^{(0.94 \pm 0.08)}$ as S wave quality factor within 105km, is obtained indicating that the region is possibly heterogeneous as well as seismically active. In addition, presence of a kink is observed at around 105km hypocentral distance while correlating path attenuation with the hypocentral distance, indicating the presence of Moho discontinuity in the region. In the second step of inversion, site amplification curves are developed separately from the attenuation corrected data for horizontal and vertical components of the accelerograms. The amplification function and predominant frequency of each recording station based on generalized inversion method is estimated and compared with that obtained from horizontal to vertical spectral ratio (of S wave portion of the accelerograms) method. Path attenuation and site characteristics obtained in the present study are very essential for developing regional ground motion model and for the seismic hazard assessment of the above study area.

Keywords: *Seismicity*, *Northwest Himalaya*, *path attenuation*, *site characteristics*, *Generalized Inversion*, *HVSR*

1 Introduction

The Himalayan arc extending approximately 2500km between Kashmir and Arunachal Pradesh is one among the seismically most active regions across the globe. Seismic activity of this region can be understood based on induced damages witnessed primarily during 4 great earthquakes (EQs) including 1897 Shillong EQ, 1905 Kangra EQ, 1950 Assam EQ and 1934 Bihar-Nepal EQ, occurred in the last 120 years. Based on seismic activity, the entire Himalayan belt can be subdivided into three distinct segments namely the western, the central and the eastern Himalayas (Philip, 2014). The region of the north-west Himalaya and its foothills, within India come under seismic zone IV and V as per IS 1893: 2016, indicating regions of high to very high seismicity.

Intensity of ground shaking during an EQ, at a particular site is a collective effect of source, path and site parameters. Source parameters include magnitude, fault mechanism, stress drop and rupture process. On the other hand, path parameters include geometric attenuation and loss of seismic energy due to the anelasticity of the earth and scattering of elastic waves in heterogeneous media. Similarly, site characteristics include modification of amplitude, frequency content and duration of the incoming seismic wave by subsurface medium as reaches the surface. Determinations of aforementioned EQ parameters are important for the development of region specific ground motion models, which can further be used for region/site specific seismic hazard assessment (Baro et al., 2018). Above parameters can be estimated from EQ records based on some spectral modelling or inversion approach like generalized inversion method (Andrews, 1986; Castro et al., 1990; Oth et al., 2009 etc.).

To understand the on-going seismicity of various regions within India, the Government of India has installed number of EQ recording stations. EQ records from these stations since 2004 are maintained by PESMOS (Program for Excellence in Strong Motion Studies), which is currently one of the most significant resource of ground motion records in India. At present, PESMOS manages EQ records from 300 recording stations which are distributed in the northern and northeaster parts of India as well as in the Andaman and Nicobar Islands (Kumar et al. 2012). It must be highlighted here that PESMOS database is lacking in terms of accurate information about subsurface for majority of recording stations (Harinarayan and Kumar, 2018). Site class given by PESMOS is based on physical description of surface materials, local geology following Seismotectonic Atlas of India (GIS 2000) and Geological Maps of Indian (GSI, 1998) and not based on actual field investigation (Kumar et al., 2012). In the absence of accurate information of local soil, utilizing EQ records from PESMOS database for seismic studies is a major challenge. Geophysical subsurface exploration studies on some of the recording stations in northwest Himalaya reported by Pandey et al., (2016a; b) had highlighted the flaws in site class given by PESMOS. There are recording stations classified to be on rock site but were found to be on soil sites by Pandey et al., (2016a; b). Harinarayan and Kumar (2018) also reported problems in the subsurface information given by PESMOS and attempted site classification of PESMOS recording stations

In the present study, EQ records from the region of the north-west Himalaya and its foothills within India, as obtained from PESMOS database, are analysed for estimating path attenuation and site characteristics separately, using a two-step generalized inversion of the S-wave Fourier spectra (hereafter referred to as GINV). In the first step, attenuation curves are developed using a non-parametric inversion approach (similar to Castro et al., 1990 and Oth et al., 2008). In the conventional generalized inversion method (Andrews, 1986; Hartzell, 1992), the second step of inversion calculates both site and source spectra, by inverting the S-wave (or Coda wave) spectra, corrected for the path parameter. This method however requires one or more reference sites (usually rock sites) in-order to remove the trade-off between the source and site parameters (Andrews 1986). In the absence of subsoil information for majority of recording stations managed by PESMOS as highlighted above, identifying reference site is not possible. For this reason, only the site parameters are evaluated in the second step of inversion, using a non-reference generalized inversion approach (similar to the work by Joshi et al., 2010; Harinarayan and Kumar 2017b). Further, Obtained site terms are compared with the one calculated from horizontal to vertical spectral ratios (HVSR) from the same S-wave window as used in the GINV.

This study is one of its kind, which systematically evaluates path and site parameters using a larger and regional database. Existing studies on attenuation characteristics determination for the northwest Himalaya used few EQ records that too from limited recording stations. Joshi (2006) estimated frequency independent S wave quality factor (Q_s) for the Garhwal Himalayas using 1991 Uttarkashi EQ and 1999 Chamoli EQ ground motion records from 8 recording stations. In another study, Singh et al., (2012) estimated frequency depended Q_s for the Kumaun Himalayas using 23 EQ events, from 9 recording stations by applying the extended coda-normalization method. Similarly, Negi et al., (2015), Banerjee and Kumar, (2017) and Tripathi et al., (2015) estimated Q_s for the Garhwal Himalayas. The aforementioned studies did not highlight the attenuation characteristics of the entire north-west Himalaya region.

Similar to path attenuation studies, very few studies on the determination of site characteristics from EQ records also exist for this region. Nath et al., (2002) computed site terms using the aftershocks of the 1999 Chamoli EQ, obtained from 5 recording stations located in the Uttarakhand region. Similarly, Sharma et al., (2014) estimated site parameters for the Garhwal region of Uttarakhand using EQ records in context of generalized inversion and HVSR. In another work, Harinarayan and Kumar (2017) reported a comparative study on site characteristics computed using EQ records from Tarai region of Uttarakhand using multiple analytical approaches. In another recent work, Harinarayan and Kumar (2018) computed site parameters for recording stations in the northwest Himalayas in terms of predominant frequency (f_{peak}) alone using HVSR method.

2 Study Area

Present study area includes states of Himachal Pradesh, Uttarakhand, Punjab, Haryana and national capital city, New Delhi, covering an area between 28º N to 34º N latitude and 75.8º E to 80.5º E longitude. According to 2011 Census, the region has a population of 96 million. From seismicity point of view, major Seismotectonic features of the present study are characterized by three north-dipping thrust systems such as the Central thrust (MCT), the Main Boundary thrust (MBT) and the Himalayan frontal thrust (HFT) (Valdiya, 1981). Other tectonic features includes, the Jhelum Balakot fault, the Drang thrust, the Lesser Himalayan Crystalline Nappes, the Jammu thrust, the Vaikrita thrust, the Karakoram fault, the Jwala Mukhi thrust, and the Ramgarh thrust. Both the MCT and the MBT lie parallel to each other within western Himalayan region and were produced during the Cenozonic shortening (Malik and Nakata 2003). The HFT is the youngest active thrust separating the Himalaya region and the Indo-Gangetic alluvial plain (Kumar et al. 2009). The HFT, the MBT and the MCT have generated major EQs in this region (Philip et al. 2014).

Two of the most damage inducing EQs, in the last 120 years, in the west Himalayan regions include 1905 Kangra-Himachal Pradesh EQ (Ms=7.8) (Ambraseys and Douglas 2004) and 2005 Muzzafarbad-Kashmir EQ (Mw=7.6) (Avouac et al. 2006). Both of these EQs caused severe loss to life and property. Recent EQs of 1991 Uttarkashi (Mw=6.8) and 1999 Chamoli (Mw=6.6) had occurred on the MCT zone (Harbindu et al. 2014). The 1999 Chamoli EQ caused a huge landslide in Gopeshwar situated less than 2km northwest of Chamoli city (Sarkar et al. 2001). This EQ also caused shaking in Chandigarh and Delhi, located far away from the epicentre (Mundepi et al., 2010).

3 Database

Ground motion records used in this study consists of three components accelerograms obtained from PESMOS database available at http://www.pesmos.in/. The instrumentation used for recording EQs consists of internal AC-63 GeoSIG triaxial force balanced accelerometers and GSR-18 GeoSIG 18 bit digitizers with external GPS (Kumar et al., 2012). Further, ground motion recordings are done in trigger mode during each EQ with a sampling rate of 200 per second.

For the present analysis, ground motion records of EQs happened between 2004 and 2017, available on PESMOS are used. For estimating site characteristics, 341 records from 86 EQs, with magnitudes ranging from Mw=2.3 to 5.8, having focal depths ranging from 2 to 80km are used. Further, these records are corresponding to 101 recording stations, located in the hypocentral distance ranging from 9 to 355km. Coordinates of each of the recording station, used in this work are listed in Table 1, columns 2 and 3. Further, details of EQs used for estimating site characteristics are summarized in Table 2.

For estimating path attenuation however, only those EQs recorded at atleast two recording stations among which at least one recording station is located within hypocentral distance equal to or less than the reference distance (reference distance is discussed under section 'Spectral attenuation with distance) are considered. Out of 341 EQ records used for estimating site parameters, only 207 EQ records satisfies the above mentioned reference distance criteria. Final database for estimating path attenuation consists of 207 records from 32 EQs, recorded at 69 recording stations, with magnitude (Mw) in the range of 3.1 to 5.5, focal depths from 3 to 55km and hypocentral distance from 9 to 200km. Table 3 summarizes the details of the dataset used for estimating path attenuation. In addition, Figure 1 shows the source-to-recording station distance of the data set used in the present study.

3.1 Data processing

Signal to pre-event noise (all of equal window length) ratio (SNR) for all the records are computed and records with SNR≥5 (similar to Ameri et al., 2011) are considered for further analyses. All the EQ records are corrected for baseline correction following a 5% cosine taper and a band-pass filtering, between the frequency range of 0.25Hz and 15Hz, using a Butterworth filter. Further, time windows starting about 0.5s before the onset of the S wave and ending when 90% of the total seismic energy of the EQ record is reached, are separated and tapered with a 5% cosine window (Ameri et al., 2011; Bindi et al., 2009). Typical lengths of the time windows for the present analysis vary from 4 to 15s. Further, for some of the records, where the window lengths obtained to be longer than 15s, are fixed to 15s in order to minimize coda wave energy in the analysing time window (Oth et al., 2008). Later, based on the extracted windows, the Fourier amplitude spectra is calculated for each EQ record, smoothened by applying the Konno and Ohmachi (1999) algorithm, with the smoothing parameter "b" = 20.

For further analyses, path and site parameters are estimated using above processed EQ records, based on two separate inversion procedures as discussed separately in the following sections.

4 Path attenuation

In the first step of inversion, path attenuation curves are developed by eliminating the effect of site parameter, thereby retaining only the source and path attenuation characteristics. All EQ records, irrespective of whether located on soil or rock sites can be utilized for inversion. This way, present method is very much suitable for PESMOS database where accurate subsurface information of recording stations is not available. The horizontal portion of the accelerograms (obtained by the root mean square average of the east-west and north-south components) is considered for developing path attenuation curves. Detailed discussions on the method can be found in following sub-section.

4.1 Methodology

Following Castro et al., (1990), observed spectral amplitude (acceleration) $U_{ij}(f, R_{ij})$, of EQ j, at recording station i, and frequency f can be modelled linearly as:

$$lnU_{ij}(f, R_{ij}) = lnM_i(f) + lnA(f, R_{ij}) \quad (1)$$

Here, $M_i(f)$ is a scalar, which is governed by the magnitude of the EQ (one value for each EQ). $A(f, R_{ij})$ is the attenuation function and is independent of the magnitude of EQ. Here, $A(f, R_{ij})$ incorporates both geometric spreading and anelastic attenuation variation with the hypocentral distance. It has to be mentioned here that $A(f, R_{ij})$ in Eq. (1) is not limited to a particular functional form, instead, is assumed to decay smoothly with hypocentral distance (R_{ij}) and thus take the value of unity at a reference distance (R_0), as given in Eq. 2 (Castro et al., 1990; 1996; 2003).

$$A(f, R_0) = 1 \quad (2)$$

Model given by Eq. (1) has no factor representing site effect and is contained in both $A(f, R_{ij})$ and $M_i(f)$. Any rapid undulations in $A(f, R_{ij})$ are due to the absorbed site effects (Oth et al., 2008). Two weighing factors, w_1 and w_2 are incorporated in the Eq. (1) following Castro et al., (1990). w_2 is used to smoothen the attenuation term with distance curve by supressing the undulations and thereby removing any absorbed site effects from $A(f, R_{ij})$. w_2 is used to impose $A(f, R_0) = 1$ constraint, as mentioned earlier. The value of w_1 and w_2 here is chosen reasonably such that the site effects are supressed but the change in the attenuation characteristics with distance can be observed (Oth et al., 2008). Solution to Eq. (1) in the matrix form, after incorporating weighing factors, is obtained using singular value decomposition method, (discussed in detail in Appendix A).

4.2 Spectral attenuation with distance

Figure 2 shows the number of EQ records for various hypocentral distance range considered. It can be observed from Figure 2 that there are very less EQ records available beyond hypocentral distance of 115km. For this reason, EQ records with hypocentral distance up to 115km are only considered for the determination of path attenuation. The constraint $A(f, R_0) = 1$ is applied at R_0=15km, irrespective of the frequency. The hypocentral distance range from 15 to 115km is divided into 10 bins, each bin having 10km width. Further, attenuation curves are computed for each of the selected 17 frequencies from 1Hz to 15Hz (see Table 4, column 1). Variation of attenuation curves with hypocentral distance, obtained in the present study, for the selected frequencies is depicted in Figure 3. Based on Figure 3, a general trend in which attenuation curves exhibit decay with hypocentral distance up to 105km can be observed. Beyond 105km a kink is observed as seen in Figure 3. This kink in the attenuation curves beyond 105km is very distinct and clear at lower frequencies (<5.5 Hz). Bindi et al., (2004) and Oth et al., (2011) reported a similar trend in the attenuation curves for the Umbria Marche and Japan regions respectively. Oth et al., (2011) attributed this behaviour to the combined effect of reflected or refracted wave arrivals from the Moho in Japan. Presence of Moho in the North-west Himalaya was reported by Saikia et al., (2016) based on Teleseismic receiver function analysis. Referring to Oth et al., (2011) work, presence of kink beyond 105km in attenuation curves, as obtained in this study may also be due reflected or refracted waves from the Moho. Further, detailed study in this direction can be done in the future and is beyond the presence scope of the work. Observing the attenuation curves at different frequencies as given in Figure 3, it can concluded that attenuation curves at higher frequencies (>5.5Hz) decay more rapidly compared to lower frequencies for the present study region. This observation is consistent with the findings by Castro et al., (2003) for Guadeloupe (France) and Oth et al., (2011) for Japan.

Further, for the kink observed at 105km, in case of lower frequencies, its sharpness reduces with increasing frequency, as can be observed in Figure 3. At frequencies greater than 10Hz, the kink at 105km smoothen and the attenuation curves beyond 105km for frequencies greater than 10 Hz becomes flat as observed in Figure 3. This change in the characteristics of the kink at higher frequency indicates that the arrival of waves from the Moho also get attenuated more at higher frequencies in comparison to lower frequencies.

4.3 Quality factor (Q_s) estimation

In order to estimate Q_s, inversion is repeated, however only considering records within hypocentral distance in the range 15km to 105km, where a monotonic decrease in attenuation curves with hypocentral distance is observed (see Figure 3). The attenuation curves are modelled in terms of geometric spreading $[G(f, R_{ij})]$ and quality factor (Q) in accordance with Castro et al., (1996) as;

$$A(f, R_{ij}) = G(f, R_{ij}) \left[e^{\frac{-\pi \cdot f \cdot R_{ij}}{Q.\beta}} \right] \tag{3}$$

Where, f is the frequency and β is the mean shear wave velocity in the crustal medium taken as 3.5km/s as per Mukhopadhyay and Kayal, (2003). Further, $G(f, R_{ij})$ is considered as $1/R_{ij}$ in accordance with Banerjee and Kumar (2015) for this region. For each frequency considered in this study (see Table 4), Eq. (3) is linearized by taking logarithm and corrected for the effect of $G(f, R_{ij})$ as given in Eq. (4).

$$ln\, A(f, R_{ij}) = ln G(f, R_{ij}) - \frac{\pi \cdot f}{Q.\beta} R_{ij} \tag{4}$$

Ascribed to Castro et al., (2003), Eq. 4 is written in the form;

$$a(R) = -m\,R \quad (5)$$

Where $a(R)$ and m are given as;

$$a(R) = lnA\left(f, R_{ij}\right) - \,ln\,G\left(f, R_{ij}\right) \quad (6)$$

$$m = \frac{-\pi \cdot f}{Q \cdot \beta} \quad (7)$$

Where, m in Eq. 5 represents the slope between $a(R)$ and R based on a linear least-square fit, obtained for each of the selected frequencies. Further, the Q values are estimated for the selected frequencies by substituting the value of m computed using Eq. (7). Columns 2 and 3, Table 4 list the value of m and Q with frequency (f) respectively. In order to build the frequency dependent relationship ($Q_s = Q_0\, f^n$), the value of Q is fitted as a function of frequency using a power law. In the above expression, n is the frequency dependent coefficient, which is approximately equal to 1 and varies on the basis of the heterogeneity of the medium (Aki 1980). Variation of Q against frequency as illustrated in Figure 4 gives frequency dependent Q_s for the north-west Himalayas as;

$$Q_s = (105 \pm 11)\, f^{(0.94 \pm 0.08)} \quad (8)$$

Values of n and Q_0 (in the expression $Q_s = Q_0\, f^n$) are attributed to the level of tectonic activity and degree of heterogeneity respectively, present in the region. Aki (1980) concluded higher values of n for tectonically active regions in comparison to that of stable regions. Similarly, low value of Q_0 (<200) is an indication of larger degree of heterogeneities in the medium (Joshi 2006). The values of n (=0.94) and Q_0 (=105), obtained in this study indicate that the present study region is tectonically active, characterized by higher degree of heterogeneities, in accordance with Aki (1980) and Joshi (2006).

4.4 Comparison with regional and global attenuation characteristics

As discussed earlier, numerous studies exist where path attenuation of different parts of the present study area were attempted in the past. Comparison of present results with those obtained by the previous researchers for the northwest Himalaya and Delhi region are attempted as shown in Figure 5. It can be seen from Figure 5 that the attenuation curve obtained in the present study falls in between existing attenuation curves for the different parts of the north-west Himalaya as given in the literature, [Kinnaur, (Kumar et al., 2009), Kumoan (Mukhopadhyay et al., 2010), Garhwal regions (Negi et al., 2015) and Delhi (Sharma et al., 2015)]. It has to be highlighted here that the database for the present study also includes EQ records from Kinnaur, Kumoan, Garhwal regions of the north-west Himalayas as well as from regions in and around Delhi. For this reason, the value of Q_0 and n obtained in the present study reflects an average attenuation characteristics of regions encompassing north-west Himalaya up to Delhi region but within Indian boundary.

Furthermore, the attenuation results obtained in this study is compared with some typical results obtained globally in terms of attenuation characteristics and tectonic setting as shown in Figure 6. Literature suggests low values of Q_s for tectonically active regions [e.g. Kato Japan region (Yoshimoto et al., 1993); East central Iran (Mahood et al., 2009); Egypt (Abdel 2009); and Umbria–Marche region (Lorenzo et al., 2013)].

Similarly, relatively high values of Q_s were reported for tectonically stable areas [e.g. Baltic Shield (Kvamme and Havskov 1989); Central South Korea (Kim et al., 2004) and South Eastern Korea (Chung and Sato 2001)]. Attenuation values obtained in the present study show good agreement with other studies having lower Q_s across the globe. Further, attenuation curves for the present region is also found closer to regions of high seismicity like Umbria–Marche and Eastern Iran as can be observed from Figure 6.

5 Site Effects

After estimation of path parameter as discussed in the previous section, site characteristics of the recording stations are determined in the second step of inversion. In addition to GINV, site components are also estimated using HVSR method. Detailed discussion on GINV and HVSR is given in the subsequent sections.

5.1 GINV

GINV was developed by Andrews (1986) by improvising spectral ratio method. Since then, various forms of this technique have been developed and used for estimating the seismic site characteristics by various researchers (Castro et al., 1990; Boatwright et al., 1991; Oth et al., 2008 etc.). The methodology used for estimating site characteristics in the present study is discussed here.

As per Iwata and Irikura (1988), the Fourier amplitude (acceleration) spectrum (FAS) of the i^{th} EQ recorded, at the j^{th} recording station, $U(f)_{ij}$ can be represented in the frequency domain as the product of source term ($S(f)_{ij}$), path attenuation ($A(f)_{ij}$) and site term ($G(f)_j$) as shown below;

$$U(f)_{ij} = S(f)_{ij}\, A(f)_{ij}\, G(f)_j \tag{9}$$

Further, the path attenuation term can be removed from the spectral content of the record following Andrews (1986) as;

$$U^A(f)_{ij} = \frac{U(f)_{ij}}{A(f)_{ij}} = S(f)_{ij}\, G(f)_j \tag{10}$$

The value of $A(f)_{ij}$ can be estimated using Eq. (3) and by considering Q_s as per Eq. (8), obtained in the earlier section. Further, Eq. (10) can be linearized, by taking natural logarithms on both sides as per Andrews (1986) giving;

$$lnU^A(f)_{ij} = ln\, S(f)_i + ln\, G(f)_j \tag{11}$$

Considering: $ln\, S_i = s_i(f)$, $ln\, G\,(f)_j = g(f)$ and $lnU^A(f)_{ij} = d_{ij}$j, Eq. (11) in the matrix form can be written in accordance with Joshi et al., (2010) and following the notations of Menke (1989) as;

←	1st event		→		←	nth event		→	← Site effect→						
1	2	…	m		1	2	…	m	1	2	…	m			
1	0	…	0	…...	0	0		0	1	0	…	0	$s_1(f_1)$		$d_1(f_1)$
0	1		0	…...	0	0		0	0	1	…	0	:		:
:			:		:	:		:	:	:		:	:		:
:			:		:	:		:	:	:		:	:		:
0	0	0	1		0	0	…	0	0	0	…	1	$s_1(f_n)$		$d_1(f_m)$
													$s_n(f_1)$	=	

$$
\begin{bmatrix}
 & & & & & & & & & & & & \\
\text{For } n^{th} \text{ earthquake} & & & & & & & & & & & & \\
0 & 0 & \ldots & 0 & \ldots\ldots & 1 & & \ldots & 0 & 1 & 0 & \ldots & 0 \\
0 & 0 & \ldots & 0 & \ldots\ldots & 0 & 1 & \ldots & 0 & 0 & 1 & \ldots & 0 \\
: & : & & : & & : & : & & : & : & : & & : \\
: & : & & : & & : & : & & : & : & : & & : \\
0 & 0 & \ldots & 0 & \ldots & 0 & 0 & \ldots & 1 & 0 & 0 & \ldots & 1
\end{bmatrix}
\begin{bmatrix} : \\ s_n(f_n) \\ g(f_1) \\ g(f_2) \\ : \\ : \\ g(f_m) \end{bmatrix}
=
\begin{bmatrix} \\ d_n(f_m) \\ d_n(f_m) \\ : \\ : \\ : \\ d_n(f_m) \end{bmatrix}
$$

(12)

The matrix form in Eq. (12) represents a purely under determinate system since there are $(n + 1) \times m$ parameters for '$m \times n$' data (here m is the number of sample frequency and n is the number of EQs recorded at a particular recording station). In here, Eq. (12) is solved using Moore- Penrose matrix inversion procedure (minimum norm inversion) given by Penrose, (1955) to determine $g(f)_j$ at each of the recording station.

Based on the above discussed methodology, inversions are performed for east-west, north-south and vertical components of EQ records separately to obtain the amplification curves in the frequency range of 0.25Hz to 15Hz, for each of the three components. For further calculation, the horizontal component is obtained as the geometric mean of east-west and north-south components.

5.2 HVSR

HVSR method is an extension of Nakamura (1989) technique, which is widely to assess the subsoil characteristics using recorded ambient noises. Nakamura (1989) technique is based on the assumption that the soil amplification effects are retained only in the horizontal component whereas the source and the path effects are maintained both in vertical as well as horizontal components of ground motion. Hence, the ratio of horizontal and vertical components gives an estimate of site amplification. Lermo and Chavez-Garccia (1993) extended Nakamura (1989) technique to S wave part of the accelerograms and studied the theoretical basis of the technique by numerical modelling oSV waves. Later, HVSR method was applied to EQ recordings worldwide (Luzi et al., 2011; Yaghmaei-Sabegh and Tsang 2011; D'Alessandro et al., 2012; Harinarayan and Kumar 2017a, b, 2018 etc.) to obtain the site characteristics.

Comparative studies between HVSR and other methods of evaluating site parameters reported by Field and Jacob (1995), Parolai et al., (2004), Shoji and Kamiyama (2002) Harinarayan and Kumar (2017b) etc. show that, HVSR can provide good and reliable estimate of predominant frequency. However, the above literatures also point out discrepancies in amplification levels obtained from HVSR with other methods. In order to compare the site amplification functions obtained from HVSR and GINV methods, HVSR for each station is computed considering the same S wave window as used in the GINV method. HVSR for each recording station is determined using the following steps;

1. Calculate the response spectra considering 5% damping, for all the three components (north-south, east-west and vertical) of ground motion records.
2. Obtain the geometric mean of the two horizontal response spectra components (H) using Eq. (13) given below;

$$H = (H_{EW} \times H_{NS})^{0.5} \quad (13)$$

3. Calculate the ratio of H to V (H/V).

Where, H_{EW} and H_{NS} are the response spectrum of the horizontal east-west and north-south components respectively and V is the response spectrum corresponding to vertical component of ground motion. Then, the HVSR at each of the recording station can be estimated as;

$$(\mathrm{HVSR})_i = \frac{\sum_{i=1}^{Ni} \frac{H}{V}}{N_i} \quad (14)$$

Here, N_i is the number of events recorded at recording station "i" and $(\mathrm{HVSR})_i$ indicates the average HVSR value for a particular recording station "i". The f_{peak} is the value of frequency corresponding to a maximum value of HVSR_i (denoted by A_{peak}) at the recording station "i".

5.3 Site Parameters

Site amplitude (SA) curves are developed using GINV for the horizontal (GINV H) and the vertical components (GINV V). Figure 7 shows typical amplification curves obtained for GINV H (indicated by dashed lines) and GINV V (indicated by firm lines) for typical 6 recording stations. In general, obtained amplification values for GINV H is greater than GINV V for all frequencies. A typical observation (from Figure 7) for both GINV H and GINV V is that the high level of amplification is observed at high frequencies. For several recording stations, clear and distinct peak in the amplification curve can be observed (e.g. JAMI, BAR, GHA and SND) from Figure 7. Moreover, the overall peaks of the GINV V component are usually at higher frequencies than for the GINV H component. Further, in case of few recording stations, the shift in frequency is relatively close to a factor $\sqrt{2}$ (eg. BAR and GHA). Next, Site amplification factor (SAF) is estimated based on the GINV results (denoted by GINV H/V) as the ratio of GINV H to GINV V. The value of frequency corresponding to the maximum value of SAF (denoted as A_{peak}) is f_{peak}. GINV H/V curves are compared with those estimated using HVSR method for a total of 101 recording stations. Figure 8 shows the comparison of the HVSR (indicated by dashed lines) and GINV H/V (indicated by firm line) for typical 9 recording stations from above analyses. A general observation made from Figure 8 is that both HVSR and GINV H/V show similar SAF patterns for all recoding stations in the selected frequency range. Overall value of f_{peak} obtained exhibit 1:1 matching between the two methods. However, there is trend of difference in terms of A_{peak} values. A_{peak} values obtained using HVSR are found higher compared to those obtained using GINV H/V curves. This observation is also reported in other regions (Sharma et al., 2014; Field and Jacob, 1995). The values of f_{peak} obtained using GINV H/V and HVSR are tabulated in Column 5 and 7, Table 1 respectively. Similarly, the values of A_{peak} obtained using GINV H/V and HVSR are tabulated in Column 6 and 8, Table 1 respectively. The maximum value of f_{peak} of 15Hz is observed for the recording station GGI with a value of A_{peak} of 5.3 based on GINV H/V. The maximum value of A_{peak} of 12.2, based on GINV H/V is observed for ADIB recording station at 6.3Hz. The range of A_{peak} based on HVSR varies between 1.7 and 19.4, while based on GINV H/V, the range of A_{peak} varies between 1.5

and 12.7. Similarly, of the f_{peak} based on HVSR varies between 0.4Hz and 10Hz, while based on GINV H/V, the f_{peak} varies between 0.5Hz and 15Hz.

Further, based on the value of f_{peak} obtained above, using GINV, the recording stations are classified as either rock sites or soil sites. In general, criteria based on average shear wave velocity over 30m (V_{s30}) is used for site classification. A site can also be classified based on f_{peak} values. Such an approach was used by Harinarayan and Kumar (2018) to classify the recording stations in the north-west Himalaya based on f_{peak} obtained using HVSR method, where stations having f_{peak} less than 6.35Hz were classified as soil sites and stations having f_{peak} greater than 6.35Hz were classified as rock sites. The range of f_{peak} values reported by Harinarayan and Kumar (2018) for soil and rock sites were calculated based on the range of V_{s30} based on NEHRP site classification scheme (BSSC, 2003) in accordance with the Eq. (15) (Kramer, 1996), correlating f_{peak} to soil depth (denoted by H and taken as 30m) and shear wave velocity (V_z).

$$f_{peak} = V_z/4H \quad (15)$$

Based on NEHRP classification criteria (BSSC, 2003), all the recording stations in the present are classified as either rock site or soil site as given in Column 9, Table 1. Out of 101 recording stations 10 recording stations are classified as rock sites and the rest 91 recording stations are classified as soil sites.

5.5 Relationship between GINV H/V results and V_{s30}

The value of V_{s30} are available for 8 recording stations in Tarai region of Uttarakhand and 19 stations in Delhi region from Pandey et al., (2016a) and Pandey et al., (2016b) respectively based on MASW test. These 27 recording stations coincides with recording stations where A_{peak} and f_{peak} are determined in the present study. V_{s30} (obtained from Pandey et al., 2016 a, b), f_{peak} and A_{peak} (as per present work) for above 27 recording stations are listed in Table 5. Based on the present findings, relationship between f_{peak} and V_{s30} for the 27 recording stations is proposed as shown in Figure 9a having R^2=0.71 as;

$$\log V_{s30} = (0.48)(\log f_{peak}) + (2.33) \quad (16)$$

Similarly, the relationship between A_{peak} and V_{s30} for above 27 recording stations, as obtained in the present study (see Figure 9b) is as follows;

$$\log V_{s30} = -(0.74)(\log A_{peak}) + (2.93) \quad (17)$$

A lack of correlation (correlation coefficient =0.47) between V_{s30} and A_{peak} is observed as shown in Figure 9b, which is also reported in the previous studies like Dutta et al., (2001), (2003) and Hassani et al., (2011). It can be concluded from the proposed correlations (Eqs. 16 and 17) that the value of f_{peak} increases with increase in V_{s30} whereas the value of A_{peak} decreases with the increase in V_{s30}. It has to be highlighted here that both the equations [Eqs. 16 and 17] are applicable for sites having f_{peak} in the range 1.8 to 6 Hz, and A_{peak} in the range 2 to 6.9.

Conclusion

In the light of on-going seismicity and catastrophic damages witnessed in the past, determination of path attenuation as well as site characterization of EQ recording stations of PESMOS located in the north-west Himalayas and adjoining area is attempted. EQ recorded between 2004 and 2017 are used in the analyses based on two-step inversion. While determining path attenuation, a kink at 105km hypocentral distance is observed in this work. Referring to similar observations from other regions, presence of Moho discontinuity is proposed in the region. This finding can be validated based on detailed study and is beyond the scope of present work objective. Further, based on attenuation curve obtained till 105km hypocentral distance and over wide range of frequencies, $Q_s = (105 \pm 11)\, f^{(0.94 \pm 0.08)}$ is obtained for the present study area, clearly indicating that the region is heterogeneous and seismically active.

In absence of proper geological information of PESMOS recording stations as highlighted by numerous recent studies, site classification of all the recording stations considered in this study are done based on GINV and HVSR. Based on this analysis, out of 101 recording stations, 10 are found to be located on rock while 91 stations are found to be located on soil sites. 1:1 matching for all the recording station from GINV and HVSR further enhances the confidence on present findings. Based on the findings, two empirical correlations for A_{peak} and f_{peak} with V_{s30}, are proposed.

Path attenuation and site characteristics are the key factors to be used for developing regional ground motion model. Further, with EQ catalogue known, present findings can be used for detailed seismic hazard assessment of the study area. In addition, identifying recording station whether considered recording stations are located on rock sites or soil sites will help in utilizing ground motion records for scenario based seismic hazard assessment.

Authors Contribution:

Harinarayan N H developed code generalized inversion, analyzed the records and all relevant literature review. Kumar Abhishek (AK) highlighted the importance of site characterization for PESMOS recording stations and need for the study.

Acknowledgement

The authors would like to thank the INSPIRE Faculty program by the Department of Science and Technology (DST), Government of India for the funding project ‘‘Propagation path characterization and determination of in-situ slips along different active faults in the Shillong Plateau’’ ref. no. DST/INSPIRE/04/2014/002617 [IFA14-ENG-104] for providing necessary funding and motivation for the present study.

Reference

Abdel-Fattah, A. K.: Attenuation of body waves in the crust beneath the vicinity of Cairo Metropolitan area (Egypt) using coda normalization method, Geophys. J. Int., 176(1), 126-134, 2009.

Aki, K.: Attenuation of shear-waves in the lithosphere for frequencies from 0.05 to 25 Hz, Phys. Earth Planet. Inter., 21, 50–60, 1980.

D’Alessandro, C., Bonilla, L.F., Boore, D.M., Rovelli, A., and Scotti, O.: Predominant-period site classification for response spectra prediction equations in Italy, Bull. Seismol. Soc. Am., 102(2), 680–695, 2012.

Ameri, G., Oth, A., Pilz, M., Bindi, D., Parolai, S., Luzi, L. and Cultrera, G.: Separation of source and site effects by generalized inversiontechnique using the aftershock recordings of the 2009 L'Aquila earthquake, Bull. of Earthquake Eng., 9(3), 717-739, 2011.

Andrews, D. J.: Objective determination of source parameters and similarity of earthquakes of different size, Earthquake source mechanics, 259-267, 1986.

Banerjee, S., Kumar, A.: Determination of seismic wave attenuation for the Garhwal Himalayas, India. Geosci Res 2(2):105–126, 2017.

Baro, O., Kumar, A., and Zadeh, A.S.: Seismic hazard assessment of the Shillong Plateau, India, Geomatics, Nat. Hazards and Risk, 9:1, 841-861, 2018.

Bilham, R., Larson, K., and Freymueller, J.: GPS measurements of present-day convergence across the Nepal Himalaya, *Nature*, *386*(6620), 61, 1997.

Bindi, D., Castro, R. R., Franceschina, G., Luzi, L., and Pacor, F.: The 1997–1998 Umbria- Marche sequence (central Italy): Source, path, and site effects estimated from strong motion data recorded in the epicentral area, J. Geophys. Res. B: Solid Earth, 109(B4), 2004.

Bindi, D., Pacor, F., Luzi, L., Massa, M., and Ameri, G.: The M w 6.3, 2009 L'Aquila earthquake: source, path and site effects from spectral analysis of strong motion data, Geophys. J. Int., 179(3), 1573-1579, 2009.

BSSC (2003). Building Seismic Safety Council, NEHRP recommended provisions for seismic regulations for new buildings and other structures. Report FEMA-450 (Provisions), Federal Emergency Management Agency (FEMA), Washington.

Boatwright, J., Fletcher, J. B., and Fumal, T. E.: A general inversion scheme for source, site, and propagation characteristics using multiply recorded sets of moderate-sized earthquakes, Bull. Seismol. Soc. Am., 81(5), 1754-1782, 1991.

Castro, R. R., Anderson, J. G., and Singh, S. K.: Site response, attenuation and source spectra of S waves along the Guerrero, Mexico, subduction zone, Bull. Seismol. Soc. Am., 80(6A), 1481-1503, 1990.

Castro, R. R., Fabriol, H., Bour, M., and Le Brun, B.: Attenuation and site effects in the region of Guadeloupe, Lesser Antilles, Bull. Seismol. Soc. Am., 93(2), 612-626, 2003.

Castro, R. R., Pacor, F., Sala, A., and Petrungaro, C.: S wave attenuation and site effects in the region of Friuli, Italy, J. Geophys. Res. B: Solid Earth, 101(B10), 22355-22369, 1996.

Chung, T. W., and Sato, H.: Attenuation of high-frequency P and S waves in the crust of southeastern South Korea, Bull. Seismol. Soc. Am., 91(6), 1867-1874, 2001.

De Lorenzo, S., Del Pezzo, E., and Bianco, F.: Qc, Qβ, Qi and Qs attenuation parameters in the Umbria–Marche (Italy) *region, Phys. Earth Planet. Inter. 218, 19*-30, 2013.

Dutta, U., Biswas, N., Martirosyan, A., Papageorgiou, A., and Kinoshita, S.: Estimation of earthquake source parameters and site response in Anchorage, Alaska from strong-motion network data using generalized inversion method, Phys. Earth Planet. Inter., 137(1-4), 13-29, 2003.

Geological Survey of India (GSI) (1998) Geological maps of India. Geological Survey of India, Kolkata

Harinarayan, N. H., and Kumar, A.: Site classification of the strong motion stations of Uttarakhand, India, Based on the model horizontal to vertical spectral ratio, Geotechnical Frontiers, 141-149, 2017 a.

Harinarayan, N. H., and Kumar, A.: Seismic Site Classification of Recording Stations in Tarai Region of Uttarakhand, from Multiple Approaches, Geotech. Geol. Eng., 1-16, 2017 b.

Harinarayan, N. H., and Kumar, A.: Determination of NEHRP Site Class of Seismic Recording Stations in the Northwest Himalayas and Its Adjoining Area Using HVSR Method, Pure Appl. Geophys., 175(1), 89-107, 2018.

Hartzell, S. H.: Site response estimation from earthquake data, Bull. Seismol. Soc. Am., 82(6), 2308-2327. 1992.

Hassani, B., Zafarani, H., Farjoodi, J., and Ansari, A.: Estimation of site amplification, attenuation and source spectra of S-waves in the East-Central Iran, Soil Dyn. Earthquake Eng., 31(10), 1397-1413, 2011.

IS 1893: Part 1–2016. Indian standard criteria for earthquake resistant design of structures—part 1: General Provisions and Buildings, Bureau of Indian Standards, New Delhi, India.

Iwata, T., Irikura, K.: Source parameters of the 1983 Japan Sea earthquake sequence, J. of Physics of the Earth, 36(4), 155-184, 1988.

Joshi, A., Mohanty, M., Bansal, A. R., Dimri, V. P., and Chadha, R. K.: Use of spectral acceleration data for determination of three-dimensional attenuation structure in the Pithoragarh region of Kumaon Himalaya, J. Seismolog., 14(2), 247-272, 2010.

Joshi, A.: Use of acceleration spectra for determining the frequency-dependent attenuation coefficient and source parameters, Bull. Seismol. Soc. Am., *96*(6), 2165-2180, 2006.

Kim, K. D., Chung, T. W., and Kyung, J. B.: Attenuation of high-frequency P and S waves in the crust of Choongchung provinces, central South Korea, Bull. Seismol. Soc. Am., 94(3), 1070-1078, 2004.

Konno, K., and Ohmachi, T.: Ground-motion characteristics estimated from spectral ratio between horizontal and vertical components of microtremor, Bull. Seismol. Soc. Am., 88(1), 228-241, 1998.

Kumar, A., Mittal, H., Sachdeva, R., and Kumar, A.: Indian strong motion instrumentation network, Seismol. Res. Lett., 83(1), 59-66, 2012.

Kumar, N., Sharma, J., Arora, B. R., and Mukhopadhyay, S.: Seismotectonic model of the Kangra–Chamba sector of northwest Himalaya: Constraints from joint hypocenter determination and focal mechanism, Bull. Seismol. Soc. Am., 99(1), 95-109, 2009.

Kvamme, L. B., and Havskov, J.: Q in southern Norway, Bull. Seismol. Soc. Am., 79(5), 1575-1588, 1989.

Lermo, J., and Chávez-García, F. J.: Site effect evaluation using spectral ratios with only one station. Bull. Seismol. Soc. Am., 83(5), 1574-1594, 1993.

Luzi, L., Puglia, R., Pacor, F., Gallipoli, M.R., Bindi D, and Mucciarelli, M.: Proposal for a soil classification based on parameters alternative or complementary to Vs30, Bull. Seismol. Soc. Am., 9(6), 1877-1898, 2011.

Ma'hood, M., Hamzehloo, H., and Doloei, G. J.: Attenuation of high frequency P and S waves in the crust of the East-Central Iran, Geophys. J. Int., 179(3), 1669-1678, 2009.

Mahajan, A.K. and Kumar, S.K.: Macroseismic field observations of January 26th, 2001 Kachchh earthquake and its seismotectonics, J. Asian Earth Sci., 23: 17–23, 2004.

Menke, W.: Geophysical data analysis: discrete inverse theory: MATLAB edition (Vol. 45). Academic press, 2012.

Mukhopadhyay, S., and Kayal, J. R.: Seismic tomography structure of the 1999 Chamoli earthquake source area in the Garhwal Himalaya, Bull. Seismol. Soc. Am., 93(4), 1854-1861, 2003.

Mukhopadhyay, S., Sharma, J., Del-Pezzo, E., and Kumar, N.: Study of attenuation mechanism for Garwhal–Kumaun Himalayas from analysis of coda of local earthquakes, Phys. Earth Planet. Inter., 180(1-2), 7-15, 2010.

Nakamura, Y.: A method for dynamic characteristics estimation of subsurface using microtremor on the ground surface, Railway Technical Research Institute, Quarterly Reports, 30(1), 1989.

Nath, S. K., Sengupta, P., and Kayal, J. R.: Determination of S-wave site response in the Garhwal Himalaya from the aftershock sequence of the 1999 Chamoli earthquake, Bull. Seismol. Soc. Am., 92(3), 1072-1081, 2002.

Negi, S. S., Paul, A., and Joshi, A.: Body wave crustal attenuation characteristics in the Garhwal Himalaya, India, Pure Appl. Geophys., 172(6), 1451-1469, 2015.

Oth, A., Bindi, D., Parolai, S., and Di, Giacomo, D.: Spectral Analysis of K-NET and KiK-net Data in Japan, Part II: On Attenuation Characteristics, Source Spectra, and Site Response of Borehole and Surface StationsSpectral Analysis of K-NET and KiK-net Data in Japan, Part II, Bull. Seismol. Soc. Am., 101(2), 667-687, 2011.

Oth, A., Bindi, D., Parolai, S., and Wenzel, F.: S-wave attenuation characteristics beneath the Vrancea region in Romania: new insights from the inversion of ground-motion spectra, Bull. Seismol. Soc. Am., 98(5), 2482-2497, 2008.

Oth, A., Parolai, S., Bindi, D., and Wenzel, F.: Source spectra and site response from S waves of intermediate-depth Vrancea, Romania, earthquakes, Bull. Seismol. Soc. Am., 99(1), 235-254, 2009.

Pandey, B., Jakka, R. S., and Kumar, A.: Influence of local site conditions on strong ground motion characteristics at Tarai region of Uttarakhand, India, Nat. Hazards, 81(2), 1073-1089, 2016 a.

Pandey, B., Jakka, R. S., Kumar, A., and Mittal, H.: Site Characterization of Strong- Motion Recording Stations of Delhi Using Joint Inversion of Phase Velocity Dispersion and H/V Curve. Bull. Seismol. Soc. Am., 106(3), 1254-1266, 2016 b.

Parolai, S., Bindi, D., Baumbach, M., Grosser, H., Milkereit, C., Karakisa, S., and Zünbül, S.: Comparison of different site response estimation techniques using aftershocks of the 1999 Izmit earthquake, Bull. Seismol. Soc. Am., 94(3), 1096-1108, 2004.

Penrose, R.: A Generalized Inverse for Matrices, Proc. Cambridge Phil. Soc. 51, 406-413, 1955.

Philip, G., Suresh, N., and Bhakuni, S.S.: Active tectonics in the northwestern outer Himalaya: evidence of large-magnitude palaeoearthquakes in Pinjaur Dun and the Frontal Himalaya, Current Science, 106, 211–222, 2014.

Saikia, S., Chopra, S., Baruah, S., Baidya, P. R., and Singh, U.K.: Crustal imaging of the Northwest Himalaya and its foredeep region from teleseismic events, Geomat Nat. Haz. Risk Journal, 7(4), 1265-1286, 2016.

Sarkar, I., Pachauri, A.K. and Israil, M.: On the damage caused by the Chamoli earthquake of 29 March, 1999, J. Asian Earth Sci., 19: 129–134, 2001.

Sharma, B., Chingtham, P., Sutar, A. K., Chopra, S., and Shukla, H.P.: Frequency dependent attenuation of seismic waves for Delhi and surrounding area, India, Ann. Geophys., 58(2), 0216, 2015.

Sharma, J., Chopra, S., and Roy, K. S.: Estimation of source parameters, quality factor (QS), and site characteristics using accelerograms: Uttarakhand Himalaya region, Bull. Seismol. Soc. Am., 104(1), 360-380, 2013.

Shoji, Y., and Kamiyama, M.: Estimation of local site effects by a generalized inversion scheme using observed records of 'Small-Titan', Soil Dyn. Earthq. Eng., 22(9), 855-864, 2002.

Singh, C., Singh, A., Bharathi, V. S., Bansal, A. R., and Chadha, R. K.: Frequency-dependent body wave attenuation characteristics in the Kumaun Himalaya, Tectonophysics, 524, 37-42, 2012.

Srivastava, H.N., Bansal, B.K., and Verma, M.: Largest earthquake in Himalaya: An appraisal, J. Geol. Soc. India, 82, 15–22, 2013.

Tripathi, J. N., Singh, P., and Sharma, M. L.: Attenuation of high-frequency P and S waves in Garhwal Himalaya, India, Tectonophysics, 636, 216-227, 2014.

Valdiya, K.S.: Aspects of Tectonics, Focus on south-central Asia, Tata McGraw-Hill Publishing Company Ltd., New Delhi, 319, 1984.

Yaghmaei-Sabegh, S.: Characteristics of near-source ground motions from the 2012 Varzaghan-Ahar double Earthquakes, Northwest of Iran, Nat. Hazards, 70, 1077–1097, 2014.

Yoshimoto, K., Sato, H., and Ohtake, M.: Frequency-dependent attenuation of P and S waves in the Kanto area, Japan, based on the coda-normalization method, Geophys. J. Int., 114(1), 165-174, 1993.

Appendix A

In the matrix form, following the notations of Menke (1989) and incorporating the weighting factors w_1 and w_2 , Eq. (1) can be written in accordance with Castro et al., (1990) as:

$$
\underset{(A)}{\left|\begin{array}{ccccc|ccccc}
1 & 0 & 0 & . & \ldots & 1 & 0 & 0 & . & \ldots \\
0 & 1 & 0 & . & \ldots & 1 & 0 & 0 & . & \ldots \\
. & . & . & . & \ldots & . & . & . & . & \ldots \\
1 & 0 & 0 & . & \ldots & 0 & 1 & 0 & . & \ldots \\
. & . & . & . & . & 0 & 1 & 0 & . & \ldots \\
. & . & . & . & . & . & . & . & . & . \\
. & . & . & . & . & . & . & . & . & . \\
w_1 & 0 & 0 & . & \ldots & . & . & . & . & \ldots \\
-w_2/2 & w_2 & -w_2/2 & . & \ldots & . & . & . & . & \ldots \\
0 & -w_2/2 & w_2 & -w_2/2 & \ldots & . & . & . & . & \ldots \\
. & . & . & . & \ldots & . & . & . & . & \ldots
\end{array}\right|}
\cdot
\underset{(X)}{\left|\begin{array}{c}
\ln A_1 \\ . \\ . \\ . \\ \ln A_{10} \\ \\ \ln M_1 \\ . \\ . \\ . \\ \ln M_N
\end{array}\right|}
=
\underset{(b)}{\left|\begin{array}{c}
\ln U_{11} \\ . \\ . \\ \ln U_{ij} \\ . \\ \\ 0 \\ 0 \\ 0 \\ 0 \\ .
\end{array}\right|}
\qquad (A1)
$$

The hypocentral distances of the data set is discretized into number of bins of equal widths and the value of $A(f, R_{ij})$ is computed at each bin. The width of the bins are selected such that there is almost equal number of data points in every bin. Further, $\ln A(f, R_{ij})$ versus hypocentral distance curves at each of the selected frequencies are computed solving Eq. (2) in a least square sense, using singular value decomposition method (Menke, 1989).

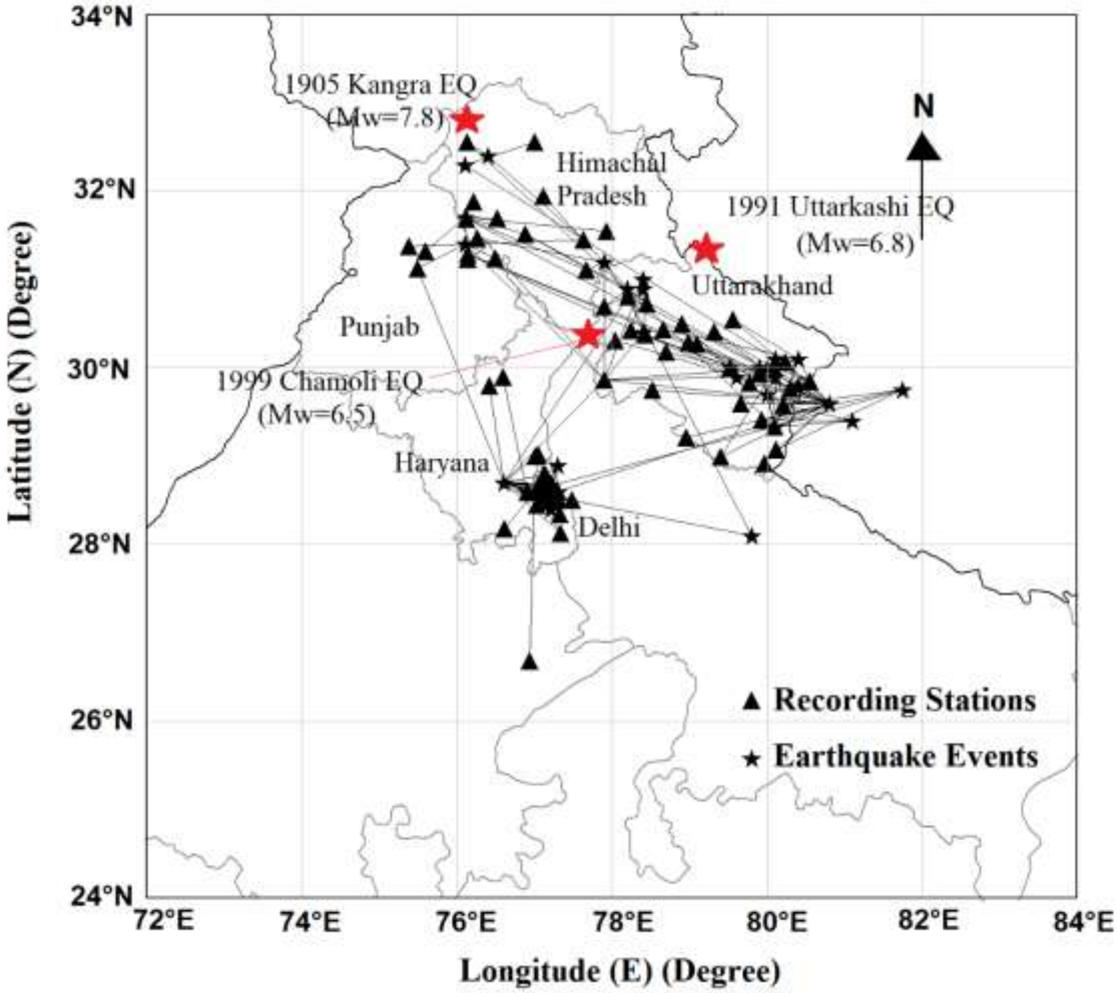

Figure 1: Map of the region under study with EQs (stars), recording stations (triangles), and paths (solid-lines).

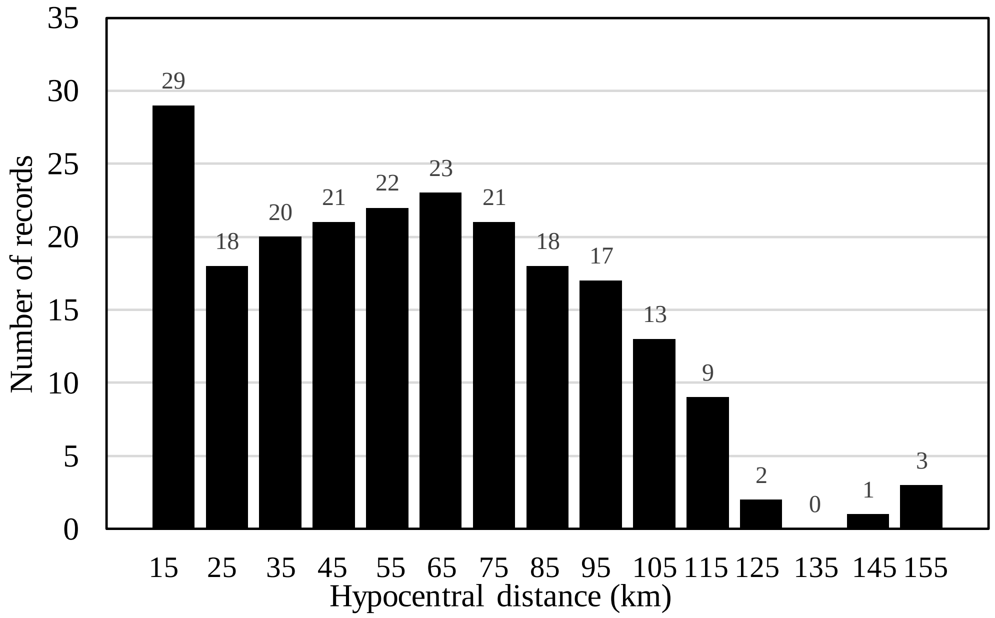

Figure 2: Distribution of hypocentral distances in the data set.

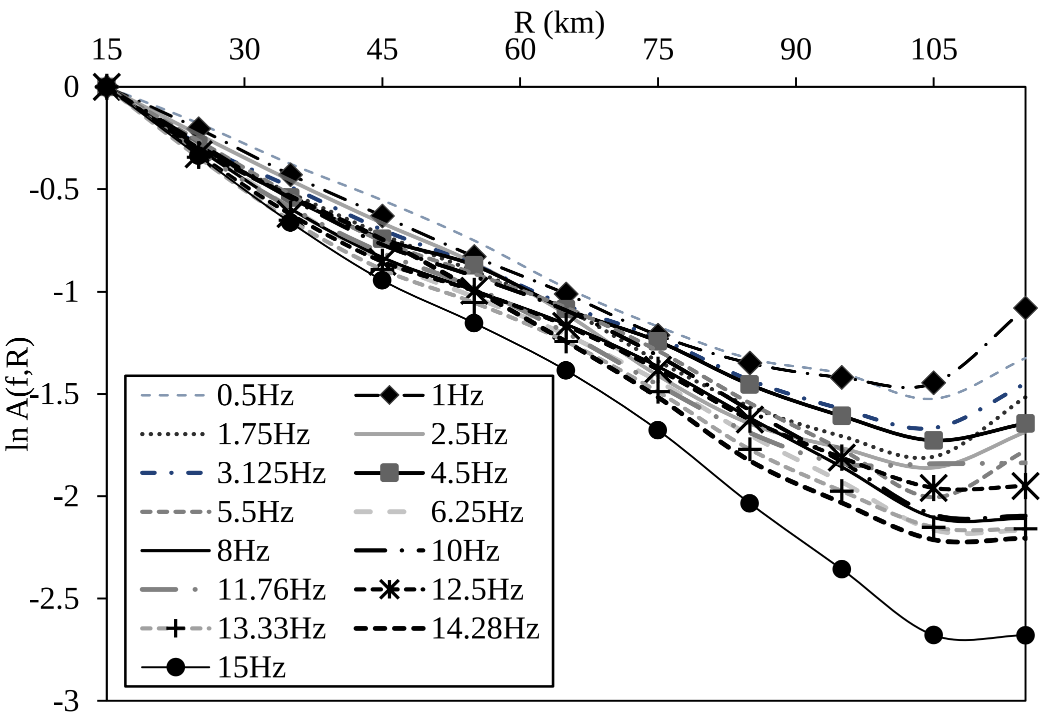

Figure 3: S wave spectral attenuation versus hypocentral distance. Note that ln A(f,R_0) at reference distance is zero.

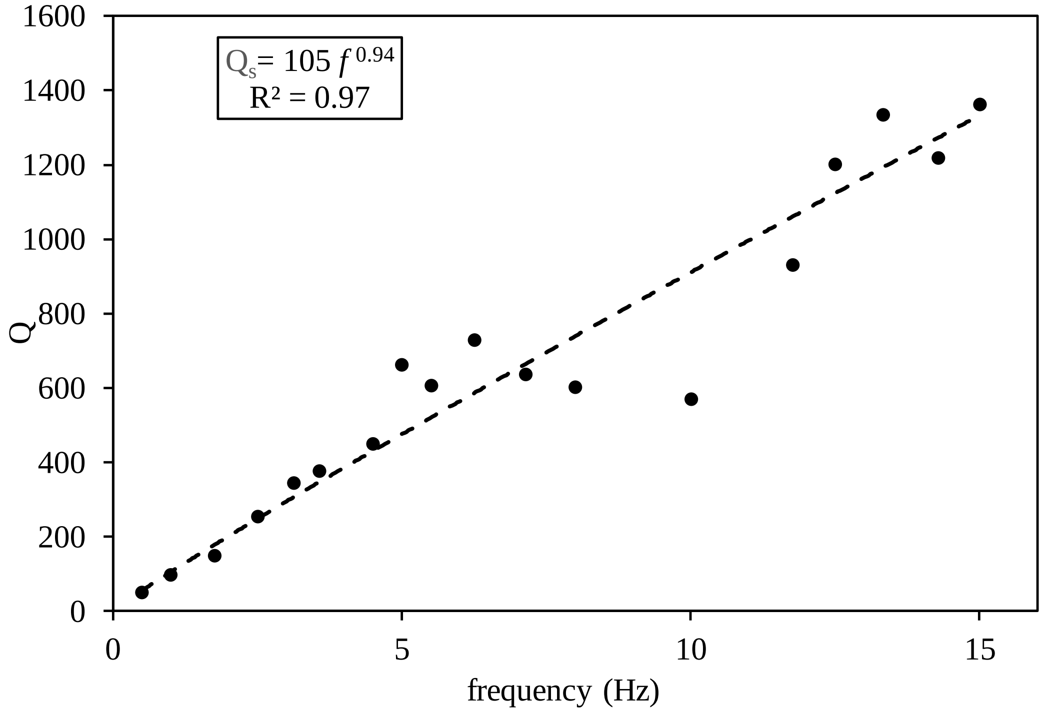

Figure 4: Frequency dependence of the quality factor Q for hypocentral distances between 15 km to 105 km

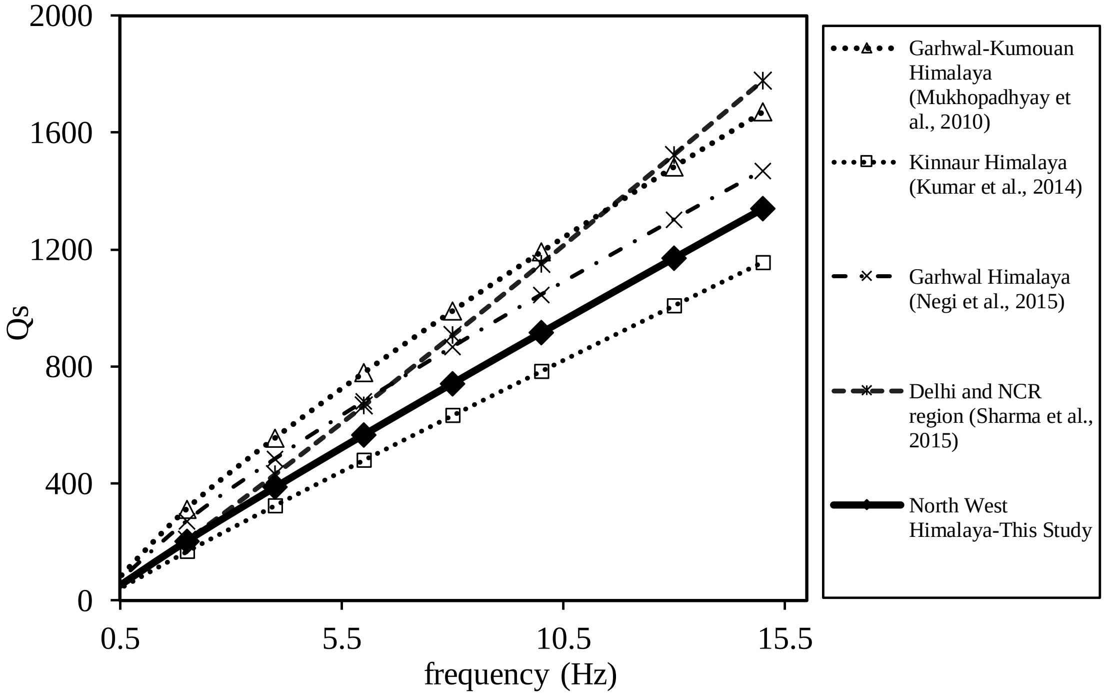

Figure 5: Comparison of Q_S values of North West Himalaya with those obtained from parts of North West Himalaya and Delhi region. The compared relations for Qs versus frequency are as follows: Garhwal-Kumouan Himalaya: $Q_S = 175 * f^{0.833}$ (Mukhopadhyay et al., 2010); Kinnaur Himalaya: $Q_S = 86 * f^{0.96}$ (Kumar et al., 2014) ; Garhwal Himalaya: $Q_S = 151 * f^{0.84}$ (Negi et al., 2015); Delhi and NCR region: $Q_S = 98 * f^{1.07}$ (Sharma et al., 2015).

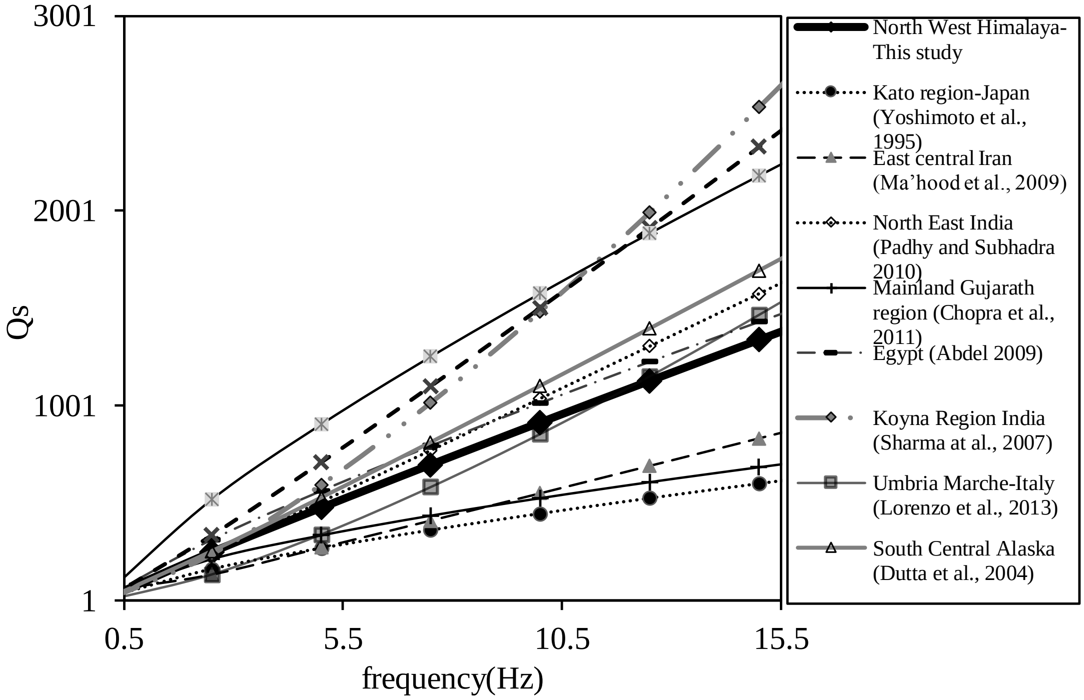

Figure 6: Comparison of Q_S values of this study with regions of different tectonic settings of the world.

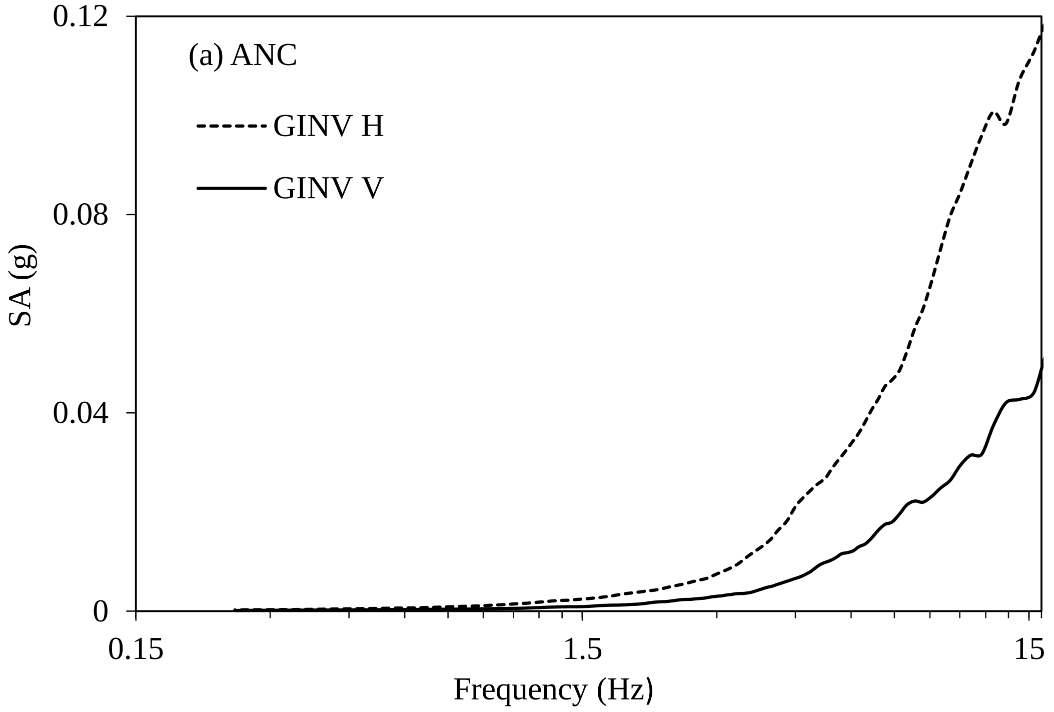

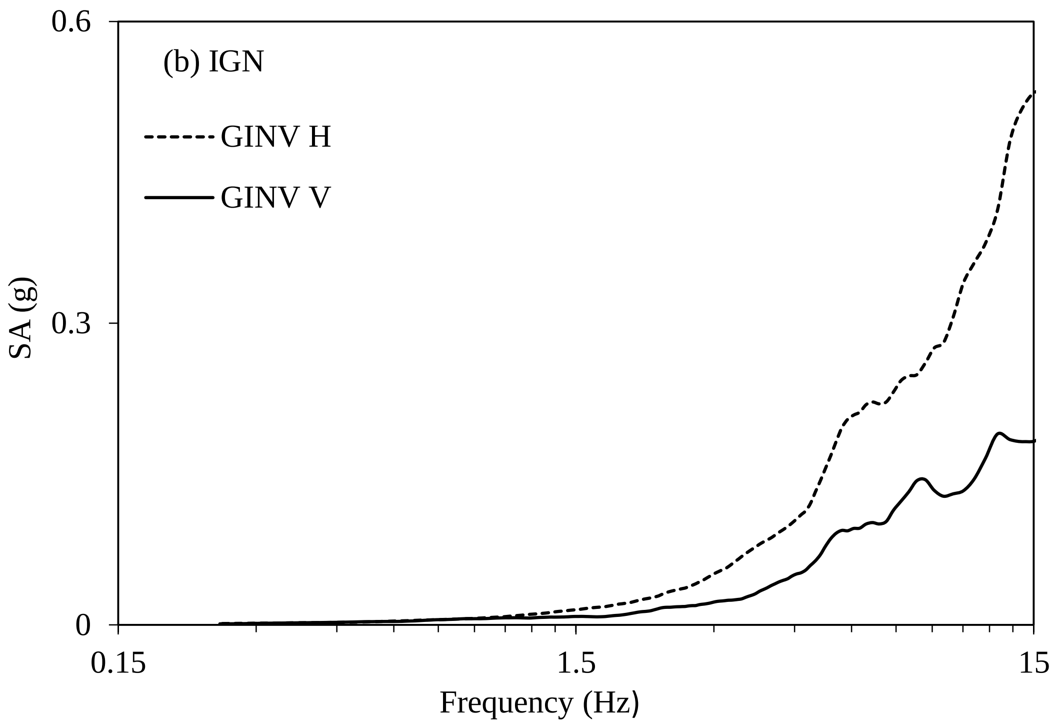

(b) IGN
GINV H
GINV V
SA (g)
0.6
0.3
0
0.15
1.5
15
Frequency (Hz)

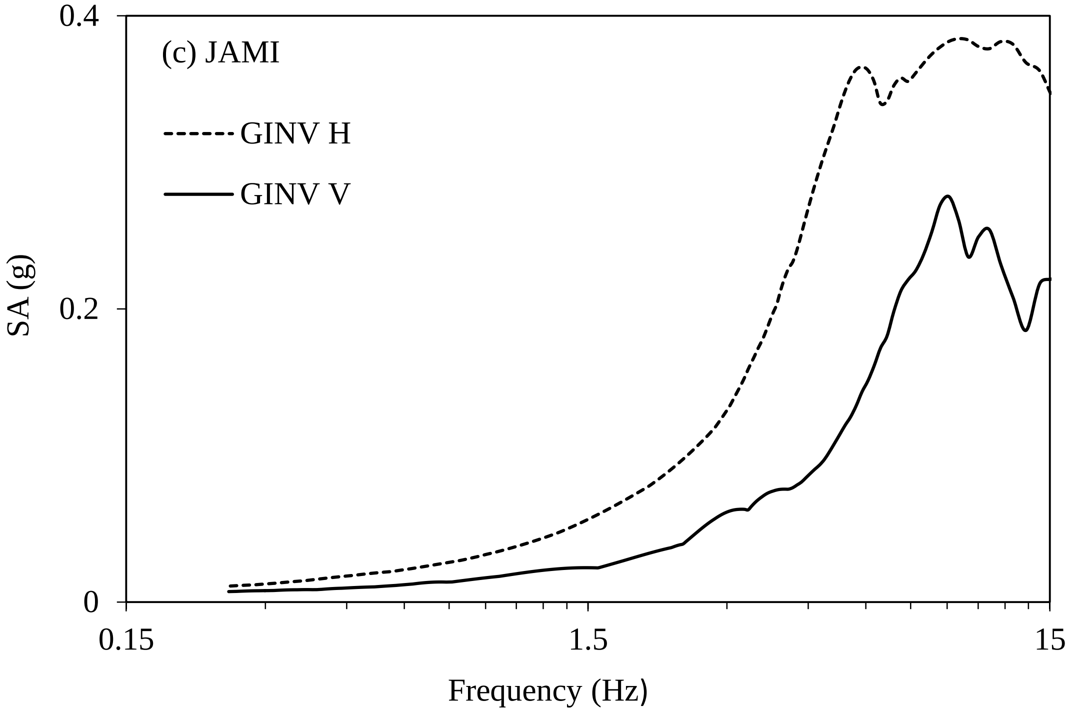

(c) JAMI
GINV H
GINV V
SA (g)
0.4
0.2
0
0.15
1.5
15
Frequency (Hz)

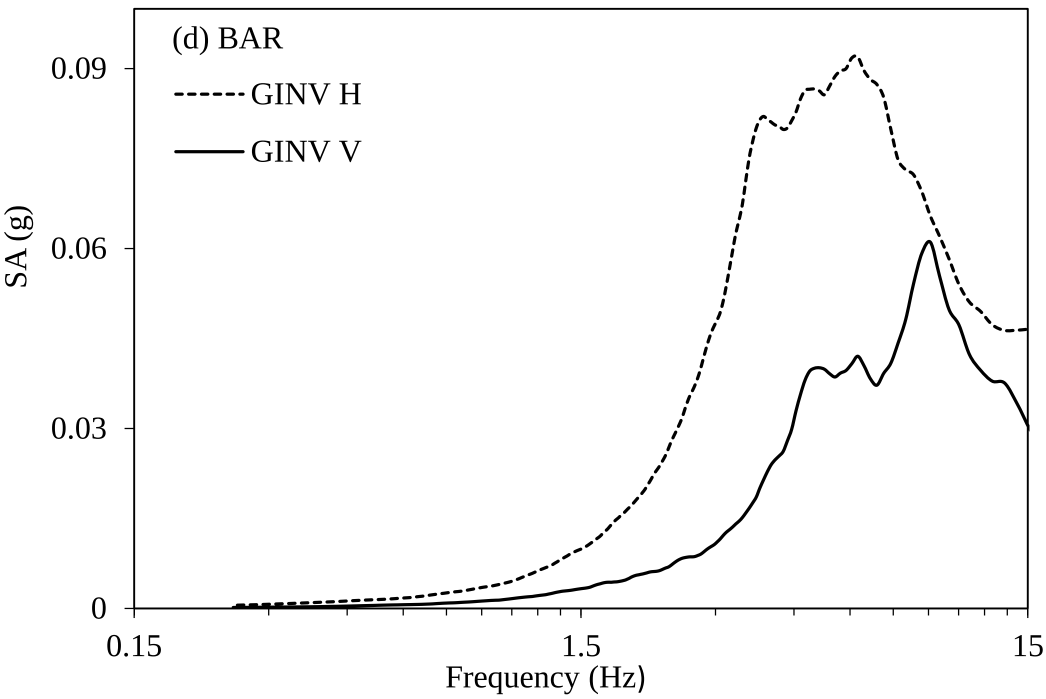
(d) BAR
GINV H
GINV V
SA (g)
0.09
0.06
0.03
0
0.15
1.5
15
Frequency (Hz)

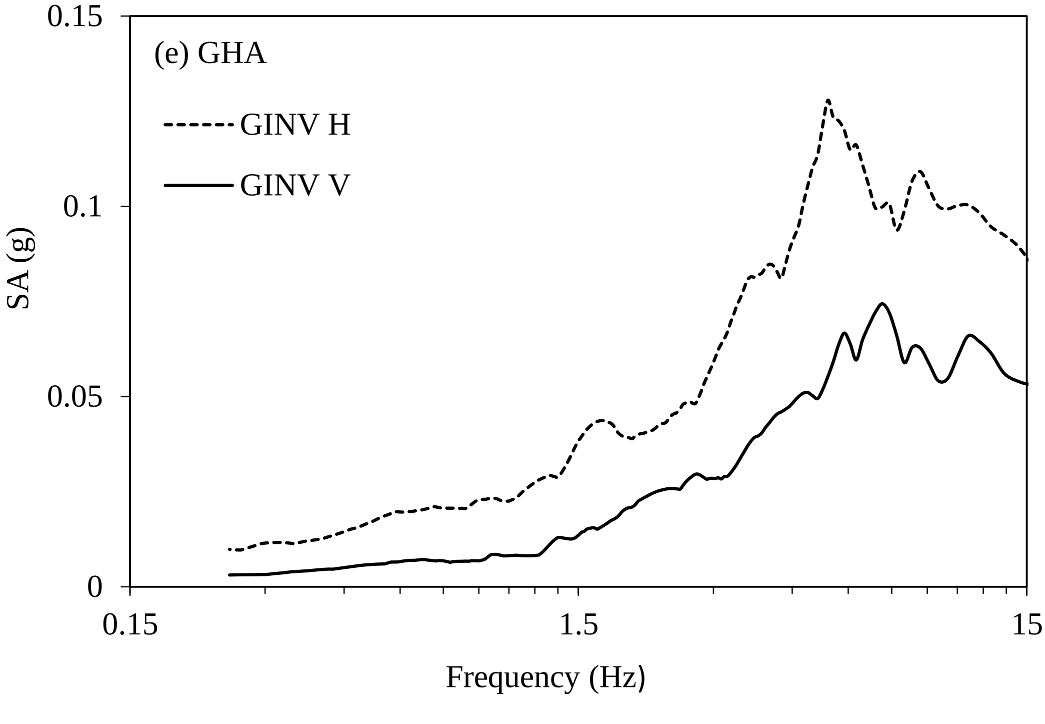
(e) GHA
GINV H
GINV V
SA (g)
0.15
0.1
0.05
0
0.15
1.5
15
Frequency (Hz)

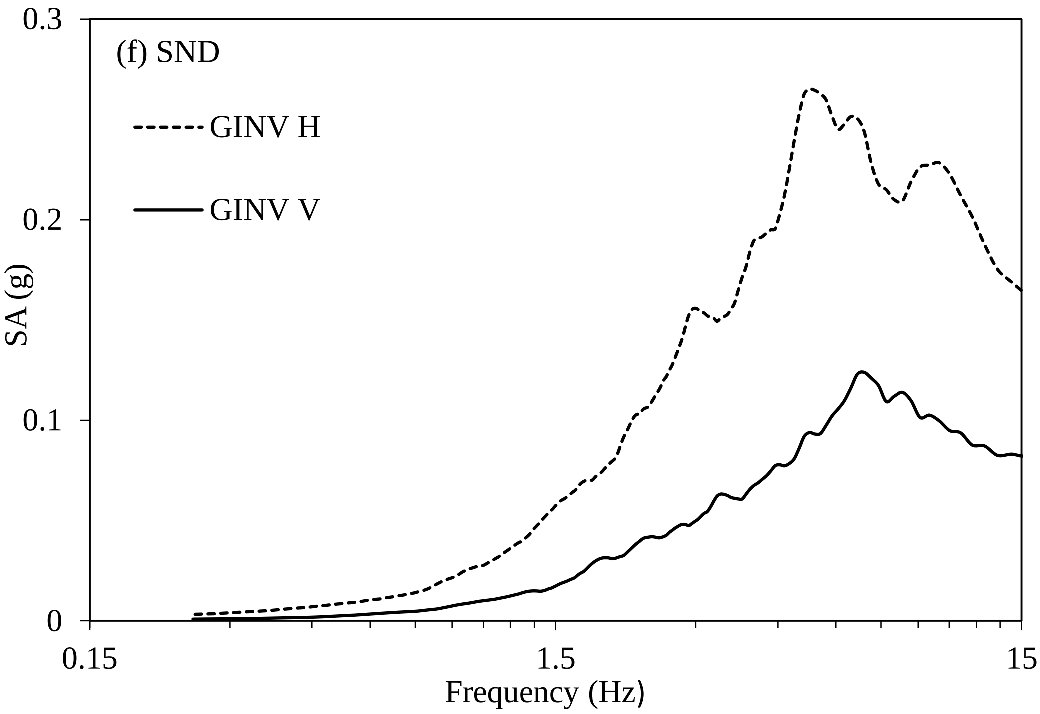

Figure 7 (a-f). Site amplitude curves obtained using GINV for horizontal component and vertical component

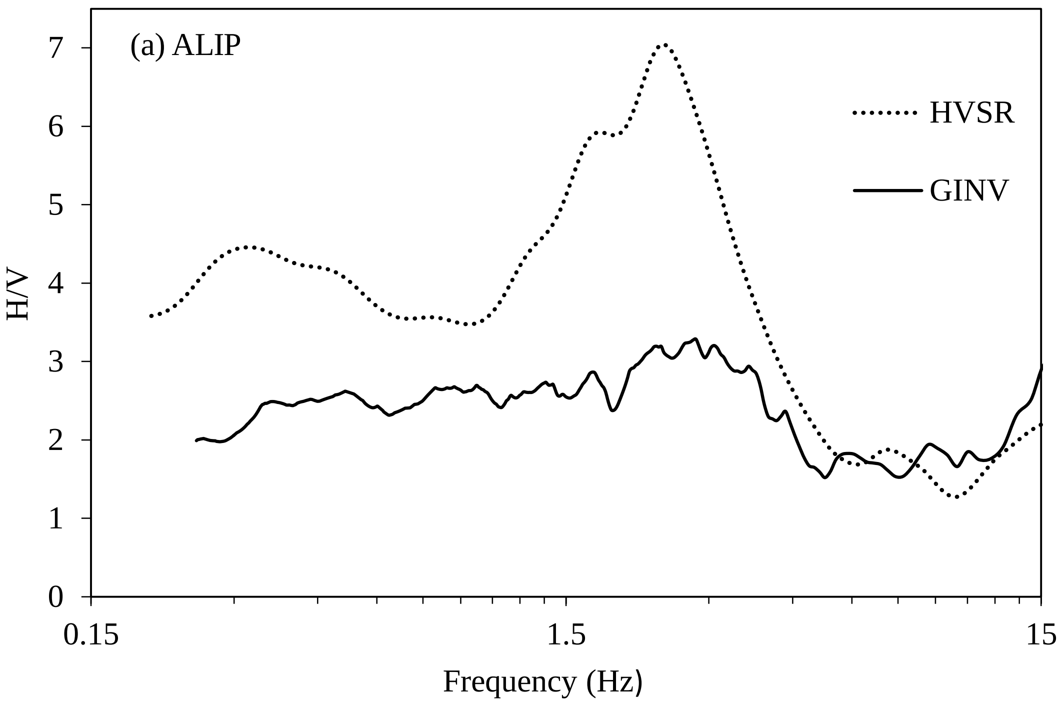

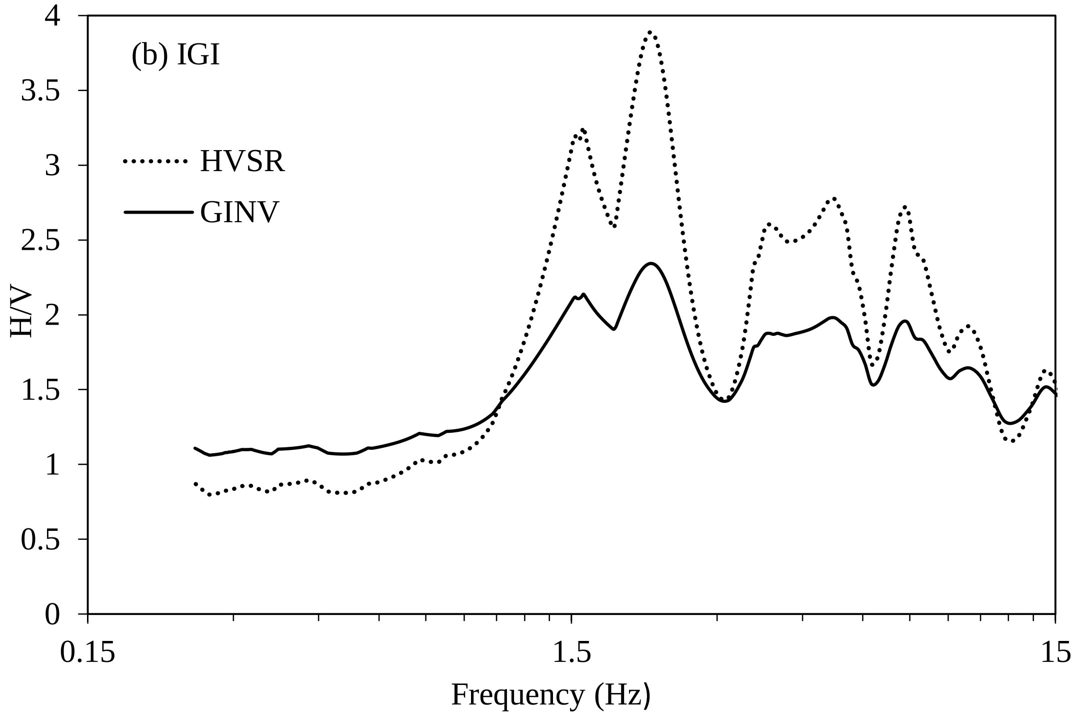
(b) IGI
HVSR
GINV
H/V
Frequency (Hz)
0
0.5
1
1.5
2
2.5
3
3.5
4
0.15
1.5
15

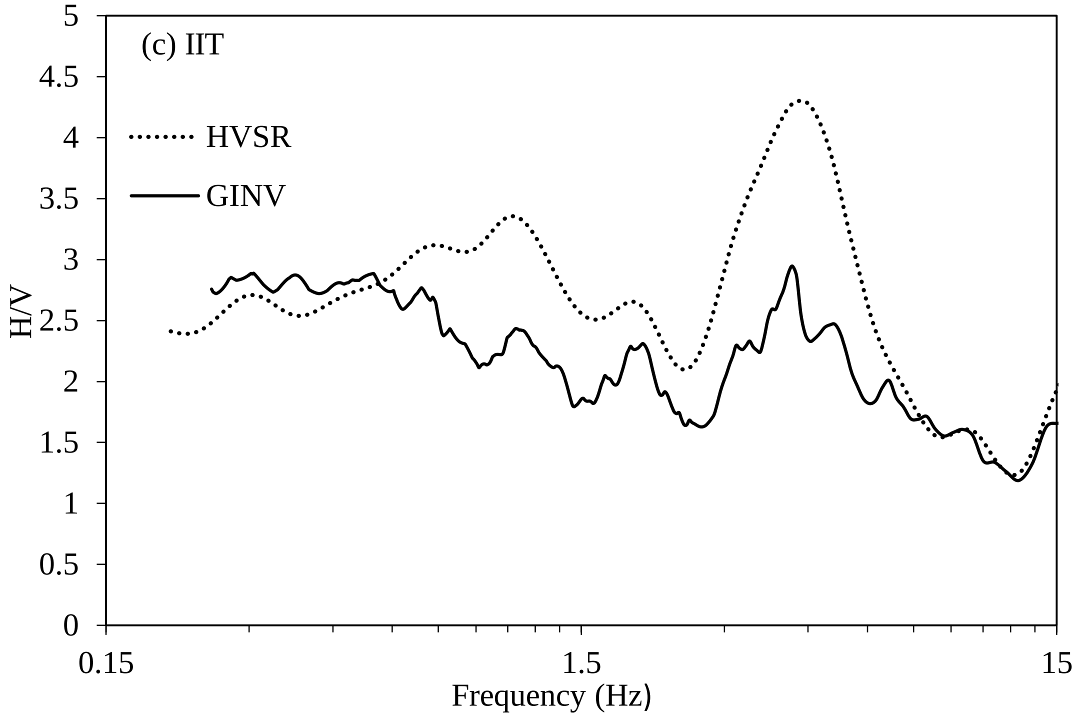
(c) IIT
HVSR
GINV
H/V
Frequency (Hz)
0
0.5
1
1.5
2
2.5
3
3.5
4
4.5
5
0.15
1.5
15

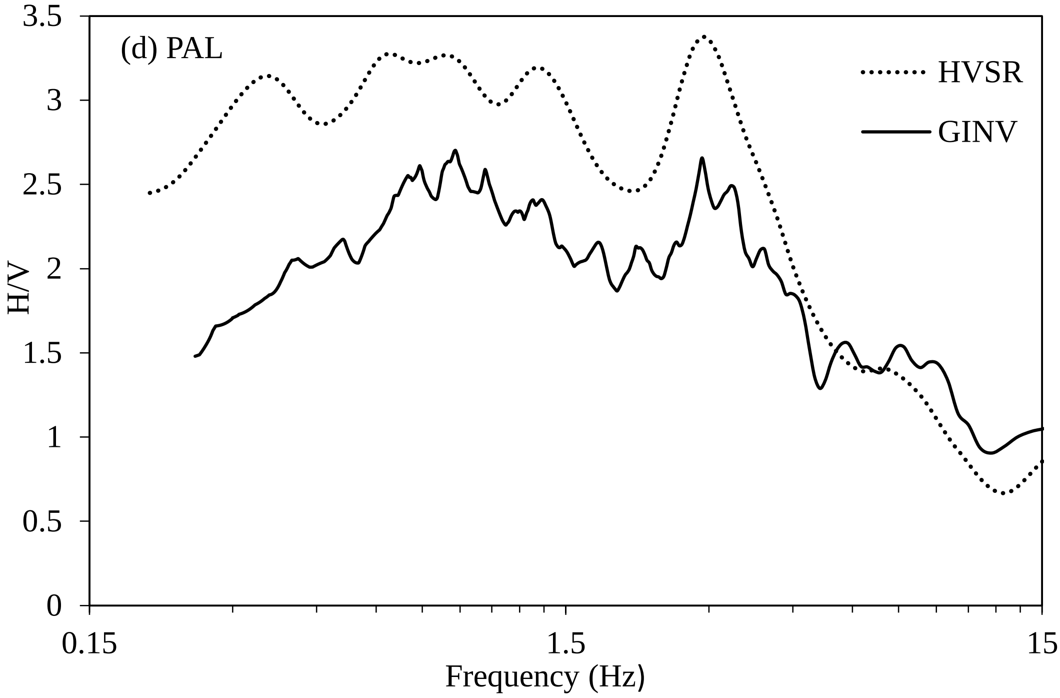
(d) PAL
HVSR
GINV
H/V
Frequency (Hz)
0
0.5
1
1.5
2
2.5
3
3.5
0.15
1.5
15

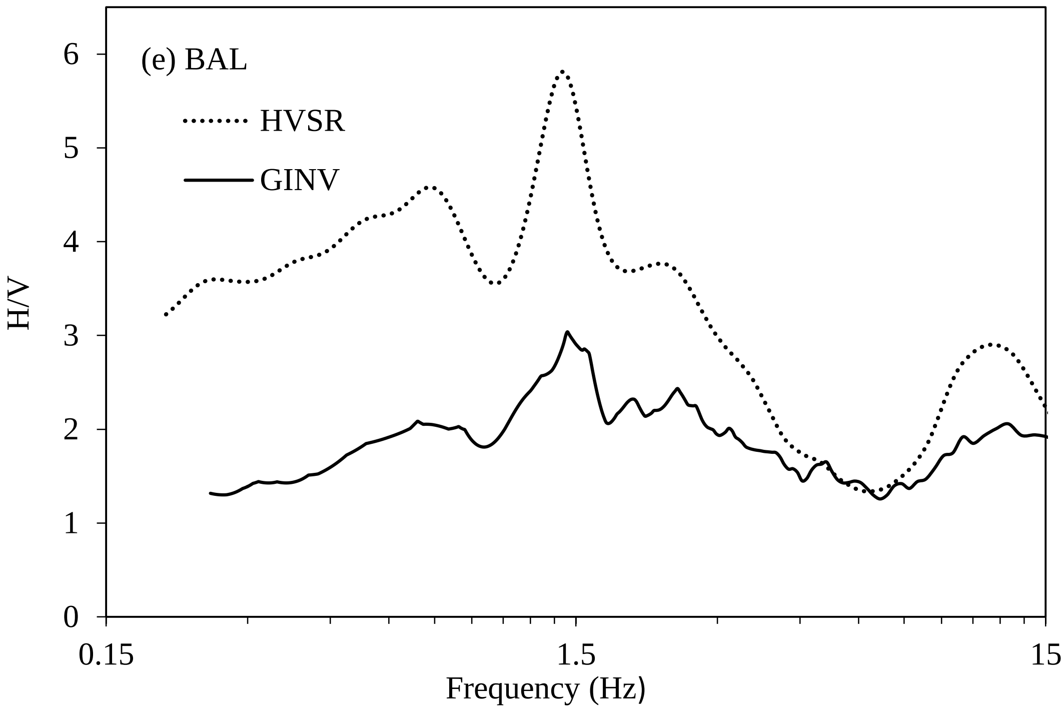
(e) BAL
HVSR
GINV
H/V
Frequency (Hz)
0
1
2
3
4
5
6
0.15
1.5
15

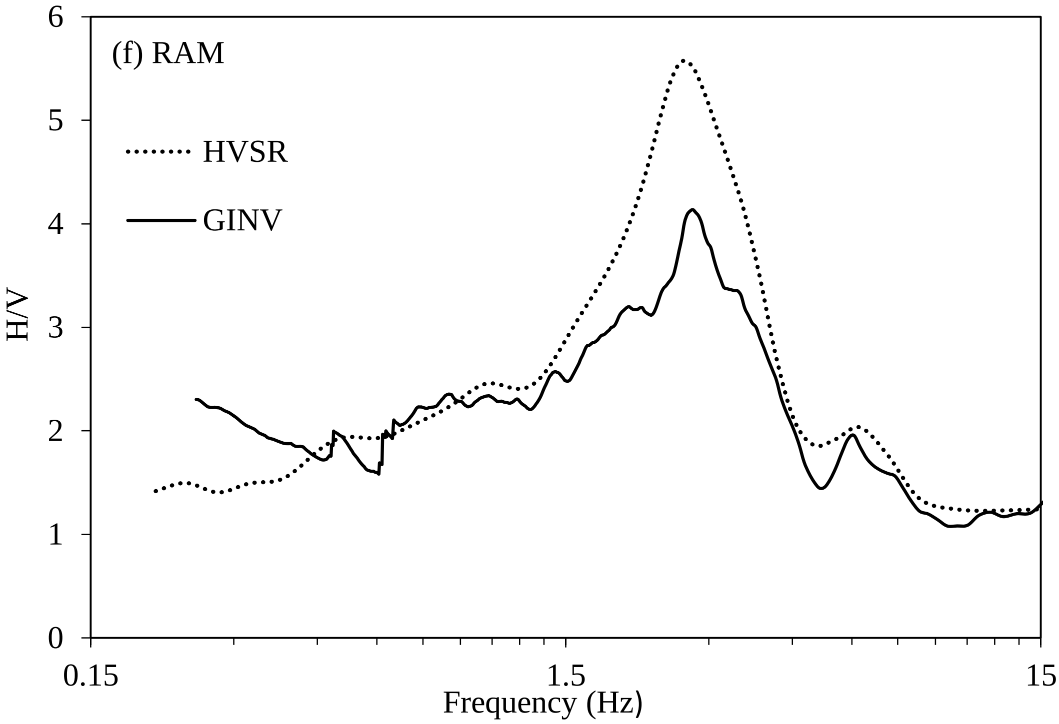
(f) RAM
HVSR
GINV
H/V
0
1
2
3
4
5
6
0.15
1.5
15
Frequency (Hz)

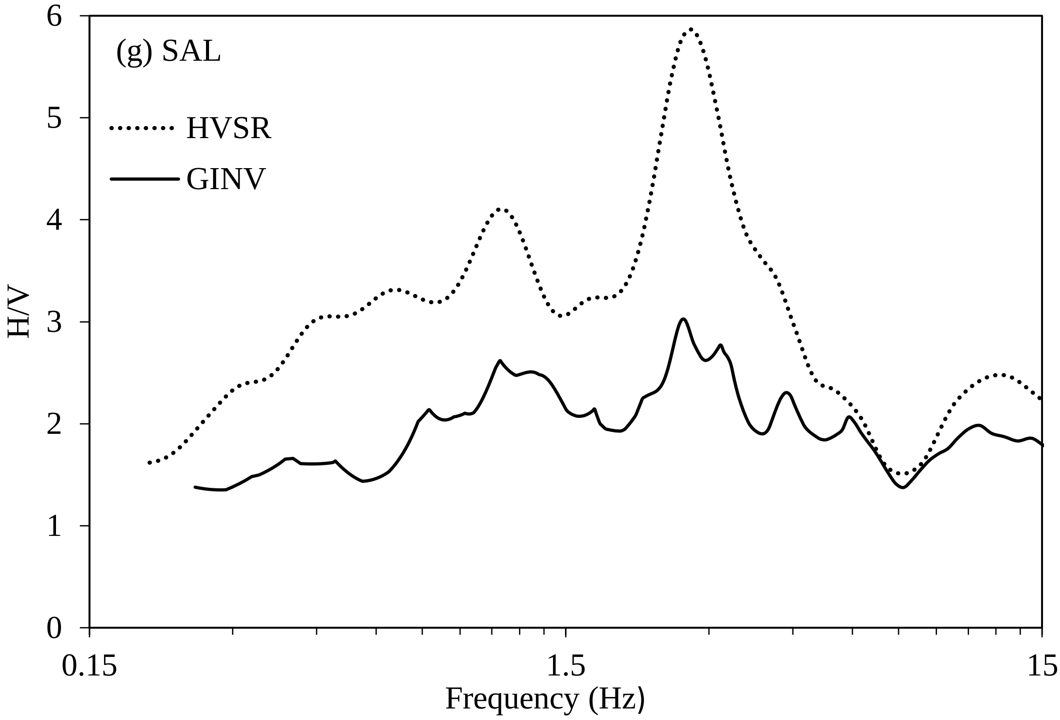
(g) SAL
HVSR
GINV
H/V
0
1
2
3
4
5
6
0.15
1.5
15
Frequency (Hz)

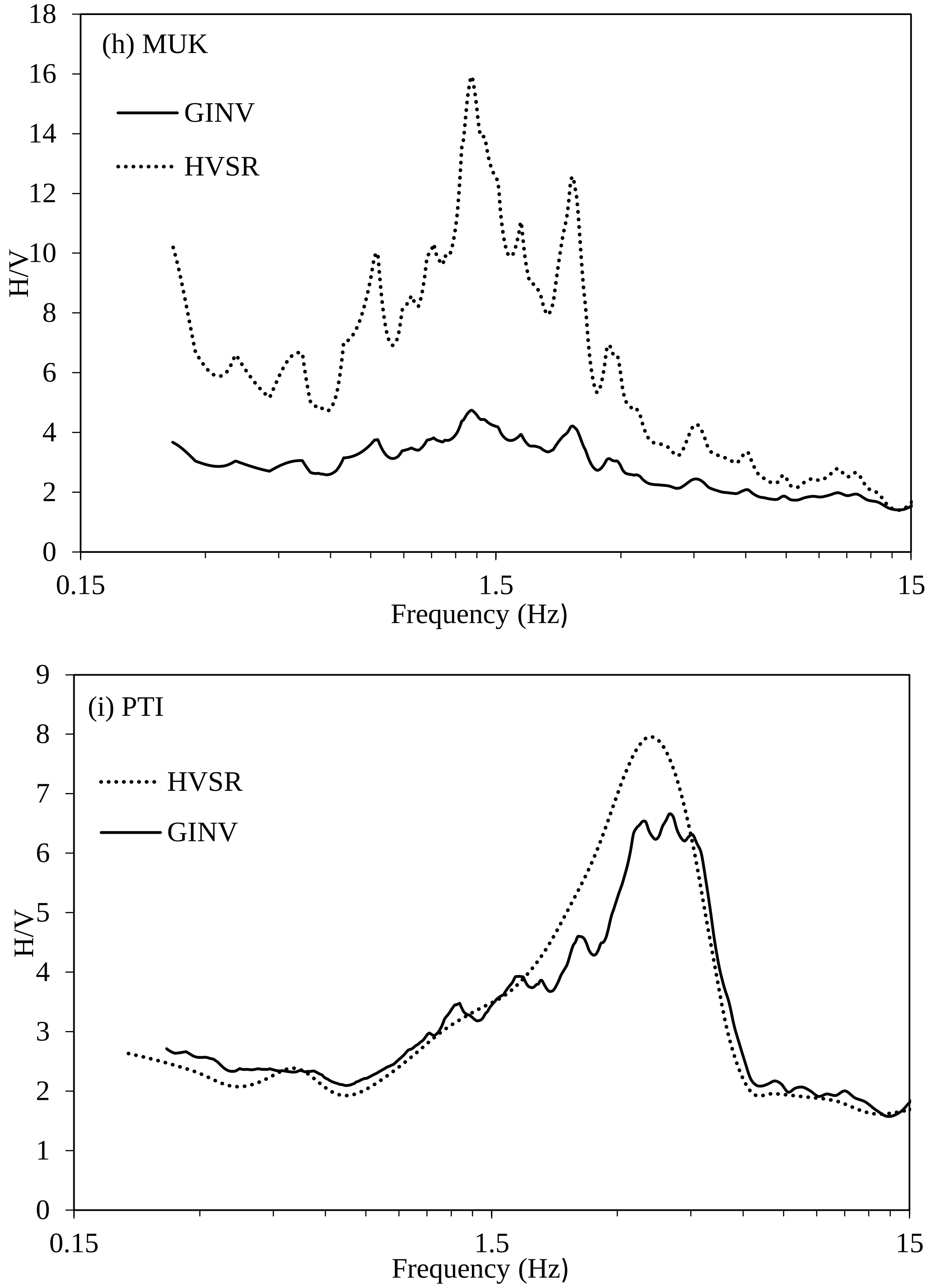

Figure 8 (a-i): Horizontal to vertical ratio curve obtained using GINV and HVSR method.

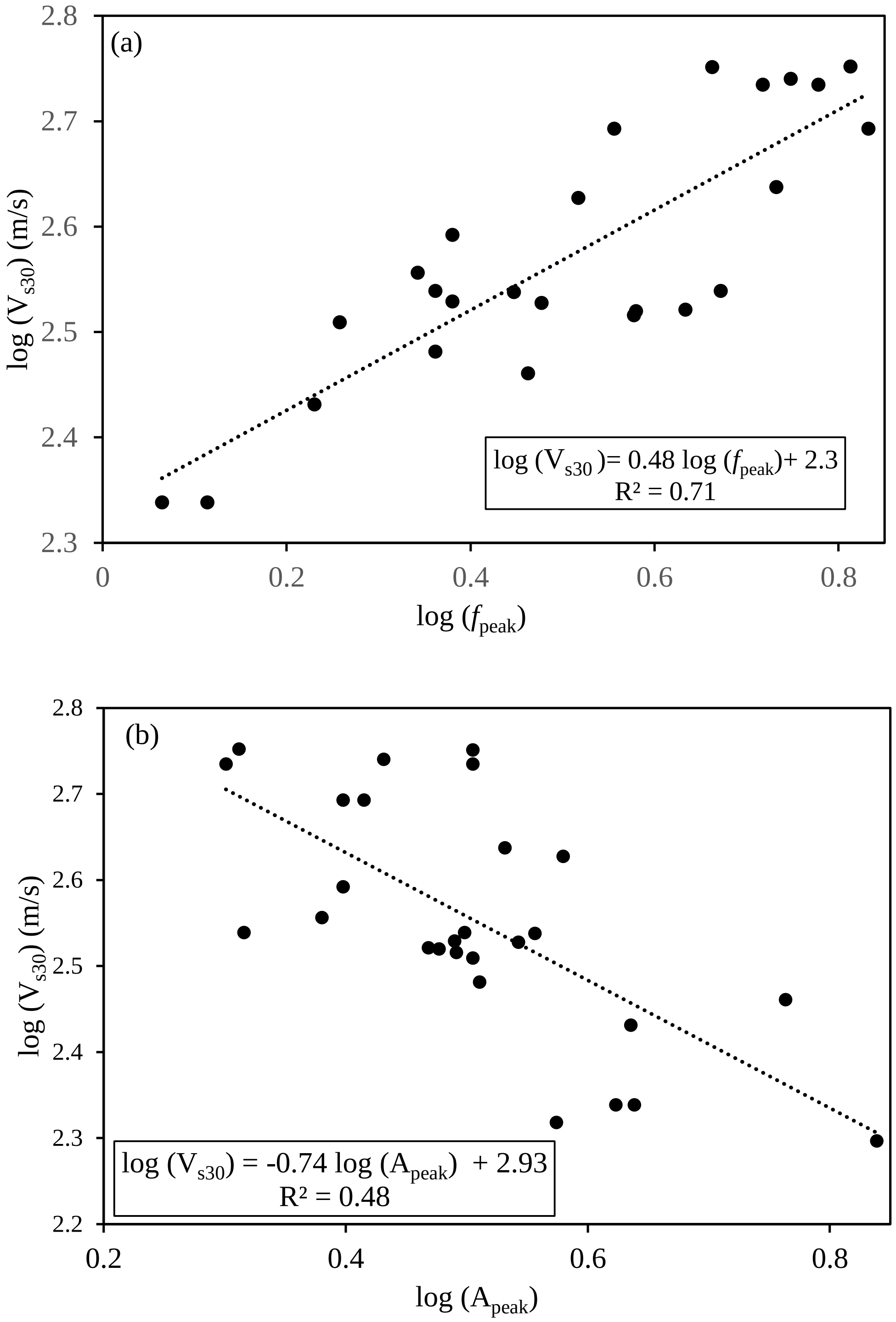

Figure 9: V_{s30} as a function of f_{peak} (a) and A_{peak} (b) of GINV method for recording stations at Delhi and Tarai region of Uttarakhand.

TABLES

Table 1: Detail of strong motion recording stations.

				GINV		HVSR							GINV		HVSR		
Si. no	Station Code	Lat.(°) (N)	Lon. (°) (E)	f_{peak}	A_{peak}	f_{peak}	A_{peak}	R* or S#	Si. no	Station Code	Lat.(°) (N)	Lon. (°) (E)	f_{peak}	A_{peak}	f_{peak}	A_{peak}	R* or S#
-1	-2	-3	-4	-5	-6	-7	-8	-9	-1	-2	-3	-4	-5	-6	-7	-8	-9
Himachal Pradesh									Uttarakhand								
1	AMB	31.7	76.1	1.7	4.3	1.2	9.3	S	1	ALM	29.6	79.7	2.1	3.0	2.8	4.4	S
2	BHA	31.6	77.9	4.5	4.0	4.1	4.4	S	2	BAG	29.8	79.8	1.5	4.7	1.5	5.2	S
3	CHM	30.4	79.3	1.4	5.4	1.5	7.5	S	3	BAR	30.8	78.2	3.0	4.5	2.8	7.0	S
4	DEH	31.9	76.2	6.8	3.5	10	5.4	R	4	CHM	32.6	76.1	3.6	2.4	2.0	2.9	S
5	DHH	32.2	76.3	2.7	4.5	2.7	4.9	S	5	CHP	29.3	80.1	5.4	5.2	5.6	6.5	S
6	HAM	31.7	76.5	2.9	3.3	3.1	6.6	S	6	CKR	30.7	77.9	2.1	3.8	2.0	4.5	S
7	JUB	31.1	77.7	5.8	3.3	5.6	4.9	S	7	CMBB	30.0	79.5	8.3	2.7	8.3	6.3	R
8	KLG	32.6	77.0	8.0	1.8	8.3	2.2	R	8	DHA	29.8	80.5	3.1	3.3	2.7	5.5	S
9	KUL	32.0	77.1	3.3	2.3	3.1	3.0	S	9	DNL	30.4	78.2	2.8	3.3	2.0	7.1	S
10	MAN	31.7	76.9	2.5	3.4	2.3	5.3	S	10	DUN	30.3	78.0	2.9	5.8	3.1	7.1	S
11	RAM	31.4	77.6	2.8	4.2	2.7	5.6	S	11	GAR	30.1	79.3	2.4	3.4	2.3	4.5	S
12	SAL	32.7	76.1	2.7	3.0	2.7	5.8	S	12	GHA	30.4	78.7	5.2	2.3	4.5	5.5	S
13	SND	31.5	76.9	5.0	3.5	5.0	4.2	S	13	GLTR	30.3	79.1	2.9	3.5	2.8	6.1	S
14	SOL	30.9	77.1	0.5	2.6	0.6	4.6	S	14	JSH	30.5	79.6	1.4	2.2	1.5	3.0	S
15	UNA	31.5	76.3	1.5	3.9	1.8	6.0	S	15	KAP	29.9	79.9	3.7	6.4	3.3	9.2	S
16	KJK	30.9	76.9	0.7	6.4	0.4	12.0	S	16	KHA	28.9	80.0	1.3	4.2	2.0	8.0	S
17	PLM	32.1	76.5	1.7	1.8	1.6	2.2	S	17	KKHR	30.2	78.9	9.5	3.5	9.5	9.3	R
Punjab									18	KOT	29.7	78.5	0.7	2.4	0.7	3.3	S
1	ANS	31.2	76.5	0.9	4.9	0.9	17.0	S	19	KSK	29.2	79.0	3.1	3.8	3.2	9.9	S
2	ASR	31.6	74.9	1.0	2.9	1.0	8.0	S	20	KSL	30.9	77.0	3.0	3.9	2.1	19.4	S
3	GSK	31.2	76.1	0.8	2.3	0.8	3.8	S	21	LANG	30.3	79.3	7.7	2.8	7.9	5.7	R
4	JAL	31.3	75.6	2.9	1.5	2.9	1.7	S	22	LAN	29.8	78.7	1.4	2.8	1.4	6.1	S
5	KAT	31.4	75.4	2.0	3.1	3.0	3.4	S	23	MUN	30.1	80.2	4.3	2.8	7.0	3.6	S
6	MOG	30.8	75.2	2.2	2.3	2.2	3.9	S	24	PAU	30.2	78.8	5.9	2.1	3.1	3.7	S
7	MUK	31.9	75.6	1.4	4.7	1.4	15.9	S	25	PTH	29.6	80.2	8.0	2.7	4.6	3.1	R
8	NAW	31.1	76.1	1.4	3.6	1.4	3.5	S	26	PTI	29.4	79.9	4.0	6.6	3.6	8.0	S
9	NKD	31.1	75.5	1.2	2.2	1.3	3.4	S	27	RIS	30.1	78.3	3.8	3.0	3.4	6.4	S
10	PHG	31.2	75.8	2.7	2.7	2.7	5.2	S	28	ROO	29.9	77.9	1.2	4.4	1.3	5.2	S
11	TAR	31.4	74.9	2.6	2.7	2.7	4.6	S	29	RUD	30.3	79.0	1.3	2.8	1.5	4.2	S
Delhi									30	SMLI	30.2	79.3	9.1	3.3	8.7	6.1	R
1	ARI	26.1	77.5	2.7	3.2	2.5	7.0	S	31	TAN	29.1	80.1	5.4	3.4	5.0	6.3	S
2	IGN	28.5	77.2	3.6	2.6	4.5	3.9	S	32	THE	30.4	78.4	1.6	2.8	1.5	3.6	S
3	JNU	28.5	77.2	9.0	2.1	8.7	3.5	R	33	UDH	29.0	79.4	2.7	6.9	2.2	10.1	S
4	DJB	28.7	77.2	2.2	3.2	10	4.5	S	34	UTK	30.7	78.4	2.4	2.9	2.3	4.4	S
5	NDI	28.7	77.2	6.8	2.5	7.2	3.7	R	35	VIK	30.5	77.8	2.3	3.8	2.3	10.4	S
6	IMD	28.7	77.2	6.0	2.0	6.3	2.9	S	36	GDRI	30.2	78.7	6.0	3.4	5.1	4.8	S
7	NTPC	28.5	77.3	2.8	3.6	2.8	5.4	S	37	TLWR	30.3	79.0	1.1	2.1	1.0	4.6	S
8	ANC	28.5	77.3	4.6	3.2	4.5	4.5	S	38	UKMB	30.3	79.1	1.0	2.9	1.4	10.0	S
9	JAMI	28.6	77.3	4.7	3.2	4.5	7.3	S	39	ADIB	30.2	79.2	6.4	12.7	6.3	17.8	R

10	LDR	28.6	77.2	0.7	4.3	0.9	7.0	S	40	NUTY	30.2	79.2	4.8	2.4	4.7	4.3	S
11	VCD	28.6	77.2	4.6	2.7	4.6	3.6	S	41	KHIB	30.2	78.8	7.7	3.3	8.0	8.7	R
12	IIT	28.6	77.3	4.3	2.9	4.5	4.3	S	42	STRK	30.3	79.0	4.7	2.8	4.7	5.8	S
13	NSIT	28.6	77.0	2.4	2.5	2.3	3.9	S	43	NANP	30.3	79.3	3.9	3.5	3.8	9.1	S
14	RGD	28.7	77.1	2.3	2.1	2.9	3.8	S		Haryana							
15	GGI	28.7	77.2	15	5.3	15	8.4	R	1	PAL	28.1	77.3	2.8	2.7	2.9	3.4	S
16	DLU	28.7	77.2	1.8	3.2	1.9	3.7	S	2	JAFR	28.6	76.9	6.0	2.0	7.1	2.6	S
17	DCE	28.8	77.1	3.8	3.1	4.7	4.2	S	3	GUR	28.4	77.0	1.0	4.1	1.0	5.2	S
18	IGI	28.6	77.1	2.2	2.4	2.2	3.8	S	4	REW	28.2	76.6	2.5	2.1	2.5	3.7	S
19	ZAKI	28.6	77.2	3.9	3.5	3.9	8.4	S	5	SON	29.0	77.0	1.0	3.5	2.8	4.0	S
20	ALIP	28.8	77.1	2.3	3.2	2.5	6.9	S	6	ROH	28.6	77.2	1.4	3.1	2.0	4.6	S
21	ROI	28.6	77.2	1.4	3.1	2.0	4.6	S	7	CRRI	29.0	77.1	4.3	3.5	4.4	9.3	S
					R*	Rock site			8	BAL	28.3	77.3	1.5	3.0	1.4	5.8	S
					S#	Soil site			9	KAI	29.8	76.4	1.2	3.0	1.2	6.5	S

Table 2: Details of earthquake events (from PESMOS) considered for estimation of site parameters in this work.

Event No.	dd/mm/yyyy	Lat.	Long.	Depth	Magnitude	Event No.	dd/mm/yyyy	Lat.	Long.	Depth	Magnitude
-1	-6	-2	-3	-4	-5	-1	-6	-2	-3	-4	-5
1	14-12-2005	30.9	79.3	25.7	5.2	44	24-09-2011	30.9	78.3	10.0	3.0
2	07-05-2006	28.7	76.6	20.2	4.1	45	26-10-2011	31.5	76.8	5.0	3.5
3	29-11-2006	27.6	76.7	13.0	3.9	46	16-01-2012	29.7	78.9	10.0	3.6
4	10-12-2006	31.5	76.7	33.0	3.5	47	12-03-2012	28.9	77.3	5.0	3.5
5	22-07-2007	29.9	77.9	33.0	5.0	48	26-02-2012	29.6	80.8	10.0	4.3
6	25-11-2007	28.6	77.0	20.3	4.3	49	27-03-2012	26.1	87.8	12.0	3.5
7	04-10-2007	32.5	76.0	10.0	3.8	50	05-03-2012	28.7	76.6	14.0	4.9
8	18-10-2007	28.3	77.6	5.6	3.6	51	28-07-2012	29.7	80.7	10.0	4.5
9	19-08-2008	30.1	80.1	15.0	4.3	52	23-08-2012	28.4	82.7	5.0	5.0
10	19-10-2008	29.1	76.9	7.0	3.2	53	02-10-2012	32.4	76.4	10.0	4.9
11	21-10-2008	31.5	77.3	10.0	4.5	54	03-10-2012	32.4	76.3	10.0	3.6
12	31-01-2009	32.5	75.9	10.0	3.7	55	06-11-2012	32.3	76.2	5.0	4.1
13	09-01-2009	31.7	78.3	16.0	3.8	56	11-11-2012	29.3	80.1	5.0	5.0
14	25-02-2009	30.6	79.3	10.0	3.7	57	15-11-2012	30.2	80.1	5.0	3.0
15	18-03-2009	30.9	78.2	10.0	3.3	58	27-11-2012	30.9	78.4	12.0	4.8
16	04-09-2008	30.1	80.4	10.0	5.1	59	19-12-2012	28.6	76.8	10.0	2.9
17	01-05-	29.	80.1	10.0	4.6	60	02-01-	29.	81.1	10.0	4.8

	2009	9					2013	4			
18	15-05-2009	30.5	79.3	15.0	4.1	61	09-01-2013	29.8	81.7	5.0	5.0
19	17-07-2009	32.3	76.1	39.3	3.7	62	10-01-2013	30.1	80.4	5.0	3.2
20	27-08-2009	30.0	80.0	14.0	3.9	63	29-01-2013	30.0	81.6	7.0	4.0
21	21-09-2009	30.9	79.1	13.0	4.7	64	11-02-2013	31.0	78.4	5.0	4.3
22	03-10-2009	30.0	79.9	15.0	4.3	65	17-02-2013	30.9	78.4	10.0	3.2
23	06-12-2009	35.8	77.3	60.0	5.3	66	01-05-2013	33.1	75.8	15.0	5.8
24	11-01-2010	29.7	80.0	15.0	3.9	67	05-09-2013	30.9	78.5	11.0	3.5
25	22-02-2010	30.0	80.1	2.0	4.7	68	11-11-2013	28.5	77.2	10.0	3.1
26	24-02-2010	28.6	76.9	17.0	2.5	69	11-11-2013	28.4	77.2	11.0	2.8
27	14-03-2010	31.7	76.1	29.0	4.6	70	11-11-2013	28.4	77.2	12.0	2.5
28	03-05-2010	30.4	78.4	8.0	3.5	71	11-11-2013	28.4	77.2	13.0	3.1
29	28-05-2010	31.2	77.9	43.0	4.8	72	16-04-2013	28.0	62.1	16.0	7.8
30	31-05-2010	30.0	79.8	10.0	3.6	73	04-06-2013	32.7	76.7	18.0	4.8
31	06-07-2010	29.8	80.4	10.0	5.1	74	05-06-2013	32.8	76.3	10.0	4.5
32	10-07-2010	29.9	79.6	10.0	4.1	75	09-07-2013	32.9	78.4	10.0	5.1
33	26-01-2011	29.0	77.2	10.0	3.2	76	13-07-2013	32.2	76.3	10.0	10.0
34	14-03-2011	30.5	79.1	8.0	3.3	77	15-07-2013	32.6	76.7	30.0	4.4
35	18-02-2011	28.6	77.3	5.0	2.3	78	02-08-2013	33.5	75.5	20.0	5.4
36	09-02-2011	30.9	78.2	10.0	5.0	79	29-08-2013	31.4	76.1	10.0	4.7
37	04-04-2011	29.6	80.8	10.0	5.7	80	20-10-2013	35.8	77.5	80.0	5.5
38	15-06-2011	30.6	80.1	10.0	3.6	81	25-12-2013	31.2	78.3	10.0	4.0
39	20-06-2011	30.5	79.4	12.0	4.6	82	17-06-2014	32.2	76.1	10.0	4.1
40	23-06-2011	30.0	80.5	5.0	3.2	83	21-08-2014	32.3	76.5	10.0	5.0
41	28-07-2011	33.3	76.0	21.0	4.4	84	29-11-2015	30.6	79.6	15.0	4.0
42	07-09-2011	28.6	77.0	8.0	4.2	85	25-09-2016	30.0	79.5	11.0	3.7
43	21-09-2011	30.9	78.3	10.0	3.1	86	01-12-2016	30.6	79.6	19.0	4.0

Table 3: List of Earthquakes and the corresponding stations considered for the estimation of path parameter.

Earthquake Event	Stations

25-11- 2007	HGR, NDI, CRRI, PAL, REW, NDI , CRRI, LDR, JAFR, IIT
19-08-2008	CHP, PTH, KAP, MUN
04-09- 2008	MUN, CHP, PTH, DHA , KAP, GHA, JSH
01-05-2009	MUN, BAG, KAP, GAR, CHM
17-07-2009	DHA, KLG
27-08-2009	KAP, BAG, MUN
03-08-2009	KAP, CHP, BAG
11-01-2010	PTH, CHP, DHA
22-02-2010	KAP, BAG, DHA, ROO, UDH
24-02-2010	RGD, IGN, ROH, DJB, CHP, ANC, JAMI, GGI, DLU, DCE
14-03-2010	DEH, JUB, SND, BHA, HAM, GAR, JAL, KAP, AMB, ROO
03-04-2010	THE, BAR, DNL, ROO
28-05-2010	JUB, BAR, ROO, UNA
06-06-2010	MUN, CHP
10-07-2010	BAG, KAP, GAR, ROO
18-02-2011	DJB, ANC
09-02-2011	UTK, SND, KUL, CKR
04-04-2011	JSH, CHP, PTI, PTH, ALM, DDH, BAG, DHA, GAR, MUN, RUD, THE, CHM, BAR, SND, KOT, DNL, LDR, ROO, TAN, KHA, UDH, KSH, DUD
12-03-2012	GGI, ANC, DLU, DCE
27-03-2012	ARI, ANC
05-03-2012	JAFR, JNU, DJB, IMD, PLW, GUR, NOI, NTPC, ANC, IIT, NSIT, ZAKI, ROO, RGD, GGI, DLU, DCE, ALIP, SON, BAR, KAI, NKD,
02-10-2012	CHA, RAM
11-11-2012	CHA, CHP, PTH
27-11-2012	UTK, THE, DNL, CKR
02-01-2013	CHP, PTI, PTH
09-01-2013	CHP, PTI, PTH, TAN
11-02-2013	UTK, ROO
11-11-2013 (19:11:18)	NTPC, IGN, JNU, DJB, IMD, VCD, IGI, RGD, GGI, DLU, DCE, ALIP
11-11-2013 (22,10,42)	IGN, JNU, DJB, VCD, RGD, DCE, ALIP
11-11-2013 (20:11:30)	IGN, JNU, DJB, VCD, RGD, GGI, DLU, DCE
29-08- 2013	GSK, RAM, ROO, NKD, ANS, KAT
25-09-2016	UKMB, CMBB, GDRI, DURD

Table 4: Resulting parameters of eq. 7.

f (Hz)	m	$Q_0 = {(\pi f)}/{(\beta m)}$
(1)	(2)	(3)
0.50	0.0095	51.65
1.00	0.0101	97.15
1.75	0.0115	149.32
2.50	0.0096	255.53
3.12	0.0089	344.54
3.57	0.0093	376.67
4.50	0.0098	450.57
5.00	0.0074	663.01
5.50	0.0089	606.39
6.25	0.0084	730.09
7.14	0.011	636.92
8.00	0.013	603.84
10.00	0.0172	570.49
11.76	0.0124	930.60

12.50	0.0102	1202.51
13.33	0.0098	1334.70
14.28	0.0115	1218.46
15.00	0.0108	1362.85

Table 5: $f_{peak,}$ A_{peak} and V_{s30} values for 27 stations located in Terai region of Uttarakhand and Delhi region.

	GINV		
Station Code	$f_{peak,}$(Hz)	$A_{peak,}$	V_{s30} (m/s)
IGN	3.6	2.6	493*
JNU	6.5	2.05	565*
DJB	5.22	3.2	543*
NDI	6.8	2.5	493*
IMD	6	2	543*
NTPC	2.8	3.6	345*
ANC	4.6	3.2	564*
JAMI	4.7	3.15	346*
LDR	0.7	4.32	270*
VCD	5.6	2.7	550*
IIT	4.3	2.94	332*
NSIT	2.4	2.5	391*
RGD	2.3	2.07	346*
DLU	1.81	3.2	323*
DCE	3.78	3.1	328*
IGI	2.2	2.4	360*
ZAKI	3	3.49	337*
ROI	2.3	3.24	303*
ALIP	1.4	3.09	338*
DUN	2.9	5.8	289**
KHA	1.3	4.2	218**
KSK	3.13	3.75	208**
RIS	3.8	3	331**
ROO	1.16	4.35	218**
TAN	5.4	3.4	434**
UDH	2.74	6.9	198**
VIK	2.29	3.8	424**

**Pandey et al., 2016a; * Pandey et al., 2016b

List of Figures

List of Tables